Materials Physics Laboratory
Department of Engineering Physics and Mathematics
Helsinki University of Technology
FIN-02015 HUT, Finland

Manipulation of Atomic and Molecular Motion with Pulsed Lasers

Pasi Ryytty

Dissertation for the degree of Doctor of Science in Technology to be presented with due permission of the Department of Engineering Physics and Mathematics for public examination and debate in Auditorium F1 at Helsinki University of Technology (Espoo, Finland) on the 29th of September, 2000, at 12 o'clock noon.

Espoo 2000

ISBN 951-22-5112-4
OTAMEDIA, ESPOO 2000

Preface

The research summarized in this work has been carried out at the Materials Physics Laboratory of Helsinki University of Technology in the department of Engineering Physics and Mathematics.

My first steps in the field of atom optics were taken under the careful guidance of Doc. Carl Aminoff. He first taught me the importance of patience, precision and carefulness in scientific work and laid the foundation on which the research of this thesis is built. To our great sorrow, he did not live to see the fruits of his ideas as he passed away after a valiant battle with a severe illness. His generous support to my work and his memory as a true scientist with a drive for exactness are well remembered and will continue to guide me in my future research work.

I wish to express special thanks to my supervisor Prof. Matti Kaivola for his continuous support to my work and for the much needed guidance in writing scientific articles. I am grateful to Prof. Martti Salomaa, the director of the laboratory, for providing funding as well as great facilities and conditions for my research work. Furthermore, my warm thanks are due to the members of the Materials Physics Laboratory for contributing to a pleasant working environment. In particular, I am much obliged to the people in the *Miilu* laboratory and remember with pleasure the good times we have spent working together.

I wish to express my gratitude to the Graduate School of Modern Optics and Photonics and the Academy of Finland for funding my doctoral studies. Personal scholarships from Emil Aaltonen foundation and Jenny and Antti Wihuri Fund are also gratefully acknowledged. The Center of Scientific Computing (CSC) is thanked for providing excellent computer resources, which were essential in the numerical studies of this thesis. Finally, I thank Seppo Kaivola and the personnel of our metal workshop for their excellent workmanship.

Espoo, May 2000

Pasi Ryytty

List of Publications

This thesis is a review of the author's work in the field of atom optics. It consists of an overview and the following selection of the author's publications in this field:

I. P. Ryytty, M. Kaivola, and C. G. Aminoff, "Deflection of Atoms by a Pulsed Standing Wave: Effects of the Laser Field Coherence", *Quantum and Semiclassical Optics* **10**, 545–553 (1998).

II. P. Ryytty, M. Kaivola, and C. G. Aminoff, "Pulsed Standing Wave Deflection of Sodium Atoms", *European Physical Journal D* **7**, 369–372 (1999).

III. P. Ryytty, M. Kaivola, and C. G. Aminoff, "Reflection of Neutral Atoms from a Pulsed Evanescent Wave", *Europhysics Letters* **36**, 343–348 (1996).

IV. P. Ryytty and M. Kaivola, "Pulsed Standing-Wave Mirror for Neutral Atoms and Molecules", *Physical Review Letters* **84**, 5074-5077 (2000).

V. P. Ryytty and M. Kaivola, "Reflection of Thermal Atoms by a Pulsed Standing Wave", *European Physical Journal D*, in press.

Throughout the overview, these papers will be referred to by Roman numerals.

Author's Contribution

The studies presented in this dissertation are the result of the research work on atom optics carried out in the Materials Physics Laboratory at Helsinki University of Technology during the years 1995–2000.

The author has played a central role in all aspects of the research work. He has developed all the theoretical methods and implemented all the numerical simulations reported in the papers I-V. All the experimental work, including the design and the construction of the apparatus, the implementation of the measurements and the data analysis, was performed by the author. Furthermore, the author has initiated the work that lead to papers I, IV and V. All the papers were written by the author.

Contents

1 Introduction

In the early 19th century, the long debate on the fundamental nature of light finally seemed to turn in favor of the wave description that Huygens had proposed already more than a hundred years earlier. The arguments and demonstrations put forward by Young, Fresnel, Arago, Fizeau and others were convincing enough to silence even the sturdiest supporters of Newton's corpuscular description of light propagation. When Maxwell then gave a solid theoretical basis for the wave description, the dispute seemed to have been settled for good. But, as we now know, the picture was not yet complete. With the advent of quantum mechanics, the corpuscular description of light re-emerged. Today we understand electromagnetic radiation to possess both particle and wave character.

According to the fundamental principles of quantum mechanics, the particle-wave duality is not a character of electromagnetic fields only. In 1924 de Broglie had suggested that all particles with mass would share this property. According to his hypothesis, the particles could be treated as waves of matter with a wavelength given by the ratio of Planck's constant to the linear momentum of the particle. This was of course in striking contradiction to the established rules of classical physics. Experimental evidence on electrons and atoms scattering in some preferred directions from crystalline surfaces soon confirmed de Broglie's suggestions [1–3]. This new insight into the character of the microworld has not only had dramatic consequences to our fundamental understanding of nature, but it has also opened up doors to completely new types of applications. In particular, it has lead to particles being used as probes in precision measurements just like light waves are used in classical optics, but often with superior results.

Although matter-wave diffraction was observed almost at the same time for electrons and atoms, optics with electron waves soon became the most promising tool for precision measurements. The success of electron optics is mainly due to the possibility to efficiently control the motion of charged particles with static electromagnetic fields. This advantage allowed electron optics to mature already in the early 1930's. For example, the first demonstration of an electron microscope was realized in 1932 [4], and a commercial version of the device appeared soon there after.

Compared with electrons, the control of the motion of atoms proved to be a difficult task, for which efficient methods have been available only for the last two decades. For a long time, problems were caused by charge neutrality of atoms, which does not allow compact atom optical components to be realized using static electromagnetic fields. For example, magnetic focusing of thermal atoms was demonstrated in 1951 by Friedburg and Paul [5, 6], but it turned out to be ineffective in practical applications. In addition to problems caused by the charge neutrality, implementation of diffractive elements for atomic beams is a challenging problem, e.g., due to the small de Broglie

wavelength of thermal atoms. Although Leavitt and Bills could observe single slit diffraction of neutral atoms in 1969 [7], it was not possible to produce efficient atom optical components until the techniques of nanofabrication were developed. In spite of these problems, the benefits of atom optics have been well known for a long time, which has kept the interest in the development of new means to control the motion of neutral atoms alive. For example, the large variety of atomic species with different masses and internal structures allows a large degree of freedom for matter-wave optics. Even the problem of charge neutrality can in fact be taken as an advantage, since it guarantees insensitivity to stray magnetic and electric fields that can otherwise cause severe problems in interferometric experiments.

During the past two decades, atom optics has experienced an explosive growth not only as regards to new components, but also in their use in practical applications. This new activity is driven mainly by the development of tunable laser sources that allow light forces to be utilized to control the atomic motion. It was shown already in the 1960's and 70's that light forces can be used to efficiently deflect [8–10], diffract [11, 12], cool [13–17], as well as trap neutral atoms [18–21]. The new results soon lead to the realization of new types of atom optical applications such as isotope separation [8, 22–24], optical levitation [25, 26], and precision laser spectroscopy [27–29]. After these early studies, more elaborate applications of light forces to control the motion of neutral atoms have emerged. The various proposals to cool and trap gas-phase atoms culminated in the development of the magneto-optical trap in 1987 [30] and in the experimental demonstration of Bose-Einstein condensation of weakly interacting atoms in 1995 [31–33]. Development of atomic beam splitters and mirrors lead to the first demonstrations of atom interferometry in the early 1990's [34–37]. Atomic lenses and collimators have provided a novel route to nanolithography [38–40], and even the first attempts on atomic microscopy have been undertaken [41]. As the tools of atom optics are improved, it is expected that the sensitivity and range of applications will further increase to cover the whole spectrum of optical applications. Already, atom lasers [42–44] and nonlinear atom optics [45] have been demonstrated to give great promise as tools for precision atom optics in the near future.

In the present day, most atom optical applications based on light forces rely on the near-resonant atom-photon interaction. Even a continuous-wave (CW) laser field can in this case provide a force strong enough to control the motion of neutral atoms. The strength of the force will, however, depend critically on the details of the internal energy-level structure of the atoms. In particular, when dealing with atoms with a rich internal energy-level structure, the light forces will, typically, be much too weak to be of any practical use. This loss of efficiency is also the main reason why experiments with molecule optics have been nearly nonexistent as compared with the rapid progress made with atoms during the past decade. In addition to the sensitivity to the internal atomic structure, the conventional methods of atom optics are, typically, capable of providing only relatively small changes in the atomic velocity. This is particularly true

if coherent control of the matter waves is required. To increase the range of applications of atom optics, new components that can provide significant changes to the atomic velocity are needed.

The main goal of this thesis is to develop new types of atom optical elements that are not limited to the low velocity regime and that can even be used to control the motion of multilevel atoms and molecules. In particular, we study the use of pulsed lasers as the light source for such components. The main advantage in using pulsed lasers lies in the increased strength of the interaction between the atom and the light field. At intensities available, e.g., from typical pulsed dye lasers, the rate of momentum transfer from the light field to the atomic center of mass can exceed 10^{10}m/s^2. The motion of atoms can thus be affected significantly even during a very short pulse of, typically, a few nanosecond duration. Also, in the case of pulsed fields the forces remain strong even at large detunings from the atomic resonance. Components based on pulsed laser fields can, therefore, be particularly useful for manipulation of multilevel atoms and molecules.

In Sec. 2 of this overview, we give a brief description of the main properties of light forces and introduce the theoretical formalism used in the later sections. We start with a classical analysis of atomic motion in a laser field that, in spite of its limitations, provides a simple description of the elementary processes related to the use of light forces. This analysis is followed by a more general description of the atomic motion needed in the study of practical components.

One of the most interesting features of atom optics is the possibility to make diffraction or interferometry experiments with matter waves. In Sec. 3 of the overview, we study the use of a pulsed standing wave as a light grating for neutral atoms. In particular, we consider the effects of the limited coherence time of a typical pulsed laser field on the momentum distribution of the deflected atoms. A simple theoretical model suitable for pulsed deflection is introduced and numerically solved for a few cases of practical interest [Paper I]. The results are compared with experimental deflection profiles of sodium atoms in Paper II.

Section 4 deals with the use of pulsed laser fields to reflect neutral atoms and molecules. The use of pulsed evanescent waves for reflection of thermal atoms is studied numerically [Paper III]. We continue by introducing a novel scheme based on a pulsed standing wave for realizing a simple reflector for neutral atoms and molecules that is insensitive to the internal structure and state of the particles. A numerical analysis of the pulsed standing-wave mirror in reflecting linear molecules [Paper IV] and thermal atoms [Paper V] is given. Finally, the main conclusions of the thesis and the possible future applications are summarized in Sec. 5.

2 Atomic Motion in an Electromagnetic Field

The effects of an electromagnetic field on atomic motion are manifested mainly through changes in the relative spatial distribution of the nucleus and the electron cloud. The detailed characteristics of these changes depend strongly on the internal structure of the atom as well as on the chosen electromagnetic field configuration. In view of manipulating the atomic center-of-mass motion, it is useful to divide the variety of possible interaction processes into two categories depending on whether energy is dissipated from the electromagnetic field or not. The first category includes processes in which the atom first absorbs energy from the field and then dissipates it in a random relaxation process, such as spontaneous emission. In this case, the atom will experience a force in the direction of the wave vector of the electromagnetic field. As will be shown below, at low intensity this force is proportional to the density of linear momentum of the electromagnetic field and is, therefore, called the *radiation pressure* force. The second category includes interactions that rely only on the stimulated emission and absorption processes. In this case, a dipole moment that oscillates in definite phase relationship with the driving field is induced on the atoms. Since the induced dipole moment is always in the direction of the electric field, atoms that move in a spatially inhomogeneous electromagnetic field will experience a force in the direction of the intensity gradient. This force is in close analogy to the force experienced by electric dipoles in a static electric field, and is thus called the *dipole force*. The direction of the dipole force can be either parallel or anti-parallel to the intensity gradient. This is a very useful property in the manipulation of the motion of neutral atoms. In particular, it allows generation of repulsive potentials that can be used, e.g., as mirrors for neutral atoms. Another key property of the dipole force is the fact that it can induce a deterministic phase shift on the atomic wave function, i.e., the coherence of the wave packet is not lost. Therefore, atom optical elements based on this force can be used for coherent control of atom beams, which is of major importance if the wave nature of the matter is to be utilized.

In general, the characteristics of the above mentioned forces, *the light forces*, depend in a rather complicated way on the coupled evolution of the internal and external degrees of freedom of the atoms. In a rigorous analysis, the related equations of motion have to be founded on the principles of quantum mechanics. Such an approach will, unfortunately, lead to rather complicated equations that do not immediately reveal the characteristics of the light forces. To illustrate the basic properties of the forces we start with a classical analysis of the atomic dynamics. This is then followed by a quantum mechanical treatment of the problem, the results of which will be applied in the later chapters of the thesis.

2.1 Classical considerations

In the classical model, atoms are considered as consisting of two oppositely charged point particles bound together by a force $\vec{F}_{\rm b}$ (see Fig. 1). If such a system is placed in an electromagnetic field, a force will be exerted on both charges, which is simply the Lorentz force appearing in classical electrodynamics, and written as

$$\vec{F} = q_i \left[\vec{E}(\vec{r}_i, t) + \dot{\vec{r}}_i \times \vec{B}(\vec{r}_i, t) \right] . \tag{1}$$

The two particles at the sites $\vec{r}_i$ have charges q_i and velocities $\dot{\vec{r}}_i$, respectively. The strengths of the electric and magnetic fields acting on the charges are denoted by $\vec{E}(\vec{r}_i, t)$ and $\vec{B}(\vec{r}_i, t)$, respectively. By transforming to the center-of-mass coordinates of the atom, we may write Newton's equation of motion for the two particles in a form where the internal atomic dynamics is separated from the center-of-mass motion. In the new coordinate system the relative position of the charges, $\vec{r}$, and their center-of-mass position, $\vec{R}$, are then given by

$$\begin{aligned} \vec{r} &= \vec{r}_1 - \vec{r}_2, \\ \vec{R} &= \frac{m_{\rm r}}{m_2}\vec{r}_1 + \frac{m_{\rm r}}{m_1}\vec{r}_2, \end{aligned} \tag{2}$$

where m_1 and m_2 are the masses of the charges and $m_r = m_1 m_2/(m_1 + m_2)$ denotes the reduced mass of the system. With the aid of the new variables, the equations of motion for the charges will transform into expressions that contain the electric and magnetic fields in the form $\vec{E}, \vec{B}(\vec{R} \pm \frac{m_i}{M}\vec{r}, t)$, where $M = m_1 + m_2$ is the total mass. At optical frequencies the electromagnetic field varies on a length scale of a few hundreds of nanometers. Since this is much larger than the typical atomic dimensions (< 1 nm), we may consider the field to be almost constant around $\vec{R}$. It is then justified to expand the field amplitudes into a Taylor series with respect to $\vec{r}$, and to retain terms up to the first order only. This is, actually, the familiar dipole approximation, which is used widely throughout the field of atomic and molecular physics. Within the dipole approximation, the equation of motion for the atomic center of mass takes the simple

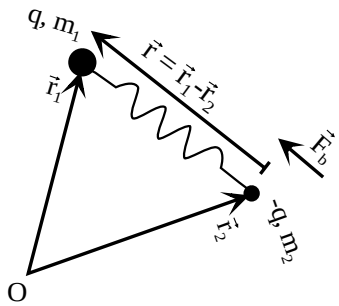

Figure 1: Structure of the classical atoms considered in the text.

form [46]

$$M\ddot{\vec{R}} = \left[\nabla\left(\vec{E}(\vec{R},t) + \vec{v}\times\vec{B}(\vec{R},t)\right)\right]\cdot\vec{\mu} + \frac{\mathrm{d}}{\mathrm{d}t}\left[\vec{\mu}\times\vec{B}(\vec{R},t)\right], \tag{3}$$

where $\vec{v}$ is the velocity of the atom and $\vec{\mu}$ is the induced dipole moment. In most cases of practical interest, the last two terms of Eq. (3) can be neglected on the basis of the following arguments: Firstly, the ratio of the electric and magnetic fields is, typically, on the order of $1/c$, and thus the second term is negligible as compared with the first term. Secondly, the total time derivative of the rapidly oscillating function averages out in the time scale of the translational motion of the atom. Under these conditions, the light force acting on the atom is then simply

$$\begin{aligned} \vec{F} &= \nabla\vec{E}(\vec{R},t)\cdot\vec{\mu} \\ &= (\vec{\mu}\cdot\hat{\epsilon})\,\nabla E(\vec{R},t). \end{aligned} \tag{4}$$

The second form of the equation follows if the polarization direction of the electromagnetic field $\hat{\epsilon}$ does not depend on position.

From Eq. (4) it is seen that the force exerted on the atom is proportional to the induced dipole moment and to the gradient of the electric field. In the following, we consider a monochromatic electromagnetic field with a spatially inhomogeneous amplitude, i.e.,

$$\vec{E}(\vec{R},t) = \frac{1}{2}\hat{\epsilon}E_0(\vec{R},t)e^{i(\vec{k}\cdot\vec{R}-\omega t)} + \text{c.c}, \tag{5}$$

and assume that the induced dipole moment depends linearly on the electric field. In the complex notation, the dipole moment can then be written in the simple form $\vec{\mu} = \alpha(\omega)\vec{E}(\vec{R},t)$, where $\alpha(\omega)$ is the atomic polarizability. By substituting the real parts of $\vec{\mu}$ and the gradient of the electric field into Eq. (4), the force exerted on the atom comes out with two components,

$$\vec{F} = \vec{F}_{\mathrm{rad}} + \vec{F}_{\mathrm{dip}}, \tag{6}$$

where

$$\vec{F}_{\mathrm{rad}} = \frac{1}{2}\alpha_{\mathcal{I}}(\omega)E_0^2(\vec{R},t)\vec{k}, \tag{7}$$

$$\vec{F}_{\mathrm{dip}} = \frac{1}{4}\alpha_{\mathcal{R}}(\omega)\nabla E_0^2(\vec{R},t). \tag{8}$$

Here $\vec{k}$ is the wave vector of the electromagnetic field, and $\alpha_{\mathcal{R}}(\omega)$ and $\alpha_{\mathcal{I}}(\omega)$ are the real and imaginary parts of the polarizability, respectively. The forces are given as averages over one oscillation period of the electromagnetic field. For atoms at rest, the following properties of the force components can immediately be identified:

- The first term of Eq. (6) is always in the direction of the wave vector of the electromagnetic field, and nonzero only when the imaginary part of the polarizability is nonzero; i.e., when energy is dissipated from the electromagnetic field.
- The second component is always in the direction of the intensity gradient of the electromagnetic field, and thus nonzero only for spatially inhomogeneous fields. Moreover, there is no net energy transfer related to the real polarizability.

The above properties indicate that $\vec{F}_{\rm rad}$ is caused by the radiation pressure exerted on the atoms in a closed absorption-spontaneous-emission cycle. On the other hand, $\vec{F}_{\rm dip}$ is analogous to the force exerted on an electric dipole in a static electric field. Since there is no net energy transfer from the electromagnetic field to the atom involved, this dipole force must be caused by redistribution of photons between the different plane wave components of the fields in the stimulated emission-absorption processes.

Let us next apply the classical electron-oscillator model to determine the dispersion relations for the polarizability components. Although the model has several shortcomings, we use it here, since it provides an easy route to deriving the main characteristics of the light forces. Within the classical model, the electron is assumed to move around the nucleus in a stable orbit. If the electron is deflected from the equilibrium distance, it will experience a harmonic restoring force, and starts to oscillate around the stationary position. Due to external relaxation processes, the oscillation is damped, and the resulting steady-state solution for the complex polarizability will be

$$\alpha(\omega) = \frac{q^2/m_{\rm r}}{\omega_0^2 - \omega^2 - {\rm i}\gamma\omega}. \tag{9}$$

Here ω_0 is the natural oscillation frequency of the dipole, and γ describes the rate of the damping. In the following we consider two important limiting cases for the polarizability; the off-resonant and near-resonant interactions.

Off-resonant interaction ($|\omega_0 - \omega| \gg \gamma$)

In the case of off-resonant interaction, the imaginary part of the polarizability in Eq. (9) vanishes. The radiation pressure exerted on the atom approaches then zero, according to Eq. (7), and is omitted in the calculations. On the other hand, by substituting the real part of the polarizability into Eq. (8), the dipole force is seen to be

$$\vec{F}_{\rm dip}^{\rm or} = \frac{q^2}{4m_{\rm r}} \frac{\nabla \vec{E}_0^2(\vec{R},t)}{\omega_0^2 - \omega^2}, \tag{10}$$

where the superscript refers to the off-resonant interaction. The above equation shows that the dipole force can be either in the direction of increasing (attractive) or decreasing (repulsive) light intensity. The sense of direction depends on whether the induced

dipole oscillates in phase ($\omega < \omega_0$) or in anti-phase ($\omega > \omega_0$) with the electric field. Also, from Eq. (10) it is clearly seen that in the limit $\omega \ll \omega_0$ the polarizability will be independent of the field frequency. In this *quasistatic case*, the dipole force has the simple form $\vec{F} = -\nabla V_{\rm eff}(\vec{R})$, where $V_{\rm eff}(\vec{R}) = -q^2\vec{E}_0^2(\vec{R},t)/(4m_{\rm r}\omega_0^2)$ is the effective potential seen by the atom in an electromagnetic field. The effective potential is the same as the Stark shift energy experienced by an atom in a static electric field, except for the factor of $1/2$ that is due to time averaging. Since the effective potential is proportional to the static polarizability, the dipole force will be relatively insensitive to the details of the internal energy-level structure of the particles. This is an important factor especially in controlling the motion of multilevel atoms and molecules, as will be seen later. Although the static polarizability of free atoms is typically rather small, the use of pulsed laser fields may allow strong enough dipole forces to be generated for an efficient control of the atomic motion. It should also be noted that, in the quasistatic case, the dipole force will always be attractive.

Near-resonant interaction ($|\omega_0 - \omega| \lesssim \gamma$)

In the case of near-resonant interaction, we may approximate the difference $\omega_0^2 - \omega^2$ by $2\omega\Delta$, where $\Delta = \omega_0 - \omega$ is the detuning of the frequency of the applied field from the atomic resonance. Within this approximation, Eq. (9) gives the following expressions for the polarizability components

$$\alpha_{\mathcal{R}}(\omega) = \frac{q^2}{m_{\rm r}\omega}\frac{\Delta}{\Delta^2+\gamma^2}, \tag{11}$$

$$\alpha_{\mathcal{I}}(\omega) = \frac{q^2}{m_{\rm r}\omega}\frac{\gamma}{\Delta^2+\gamma^2}. \tag{12}$$

The above equations show that for detunings on the order of the linewidth of the transition the real part of the polarizability experiences a strong enhancement compared with the off-resonant case, but vanishes on exact resonance. The enhanced dipole force allows efficient manipulation of the center-of-mass motion of atoms even with a relatively weak laser beam that can be obtained from, e.g., a tunable CW laser source. It is obvious, however, that this effect can be utilized only for atoms with a simple internal energy-level structure. We see from Eq. (12) that the polarizability also has a strong imaginary component and, therefore, the radiation pressure exerted on the atoms will be nonzero. The spectral line for the radiation pressure is a Lorentzian centered at the resonance frequency. This is as expected, since the absorption of photons highest on resonance.

The main characteristics of the light forces are summarized in Fig. 2. Strictly speaking, the above analysis gives only a qualitative picture of the forces for the case of weak excitation. Moreover, the classical model ascribes only one resonance frequency to the atoms, and does not include the relevant line strength. With the use of a quantum

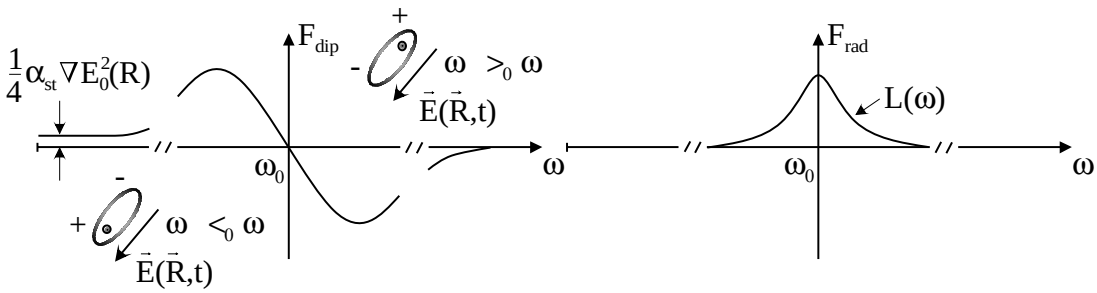

Figure 2: Properties of the light forces in the classical model.

mechanical perturbation method it is possible to improve the results of the classical model to include the whole resonance structure of the atom, and also to associate the relevant line strength to each transition [47]. The results of such an analysis will, actually, be very similar to those of the classical model. The main difference is that the polarizability of Eq. (9) should include a sum over all allowed transitions with the $q^2/m_{\rm r}$ factor replaced by $q^2 f_{\rm osc}/m_{\rm r}$, where $f_{\rm osc}$ gives the oscillator strength for each transition.

2.2 Two-level atoms

Let us next consider the atoms as simple two-level systems described by internal eigenstates $\phi_g(\vec{r})$ and $\phi_e(\vec{r})$, where g and e denote the ground and excited state, respectively (see Fig. 3). The atomic motion in an electromagnetic field can now be solved by expanding the total atomic wave function in the basis of the internal states and by solving the resulting equations of motion for the center-of-mass wave function. To compare the results with the classical model, we first neglect the phase space distribution of the atoms and concentrate only on their center-of-mass motion. This is allowed if the spread of the atomic wave packet is small in both position and momentum spaces. In this limit of a localized wave packet, Ehrenfest's theorem yields the familiar expression

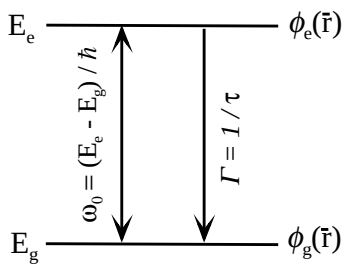

Figure 3: Two-level atom.

for the average force exerted on the atoms

$$\vec{F} = - < \nabla \hat{V} > = \nabla \left[\vec{\mu} \cdot \vec{E}(\vec{R}, t) \right]. \tag{13}$$

In the above equation, which is written within the dipole approximation, the induced dipole moment depends only on time and can be calculated using the density matrix equations of the two-level system. These equations are coupled to the center-of-mass motion through position dependent interaction terms. By using the Bloch vector formalism, the equations of motion for the atomic center of mass finally take the convenient form [48]

$$M\ddot{\vec{R}} = \frac{1}{2}\hbar \left(\mathrm{U} \nabla \Omega + \mathrm{V} \Omega \nabla \theta \right), \tag{14a}$$

$$\dot{\mathrm{U}} = (\Delta + \dot{\theta})\mathrm{V} - \frac{1}{2\tau}\mathrm{U}, \tag{14b}$$

$$\dot{\mathrm{V}} = -(\Delta + \dot{\theta})\mathrm{U} + \Omega \mathrm{W} - \frac{1}{2\tau}\mathrm{V}, \tag{14c}$$

$$\dot{\mathrm{W}} = -\Omega \mathrm{V} - \frac{1}{\tau}(\mathrm{W} + 1), \tag{14d}$$

where U, V and W are the Bloch vector components, τ is the lifetime of the excited state, and $\theta(\vec{R}(t))$ denotes the phase of the light field. The strength of the atom-photon interaction is determined by the Rabi frequency defined as $\Omega = \mu E(t)/\hbar$, where μ is the dipole matrix element for the transition. From Eq. (14a) it is seen that the force exerted on the two-level atoms consists of two components, which are proportional to the gradients of the electric field and the phase of the electromagnetic field. According to the arguments given in the previous subsection, these force components can be identified as the dipole force and the radiation pressure force. Furthermore, Eqs. (14) show that the light forces do not, in general, have an analytic position-dependent solution, but they depend on the history of the atomic trajectory. A unique position-dependent force can be obtained only in some simple cases. For example, in the case of a slowly moving atom the steady-state solution of the Bloch vector can be used in Eq. (14a) to give an expression for the light force in the simple form

$$\vec{F} = \frac{\hbar \Omega^2 \nabla \theta / \tau + \hbar(\Delta + \dot{\theta}) \nabla \Omega^2}{4(\Delta + \dot{\theta})^2 + (1/\tau)^2 + 2\Omega^2}. \tag{15}$$

At a slow excitation rate, the above expression reduces to that obtained by using the classical model, but with the oscillator strength included. Equation (15) also tells us that the radiation pressure exerted on the atoms by a plane wave is of the form $F = \hbar k R_{21}$, where R_{21} is the rate of spontaneous emission. This confirms the interpretation of the radiation pressure as resulting from the net recoil experienced by an atom in a closed absorption-spontaneous-emission cycle.

Equations (14) are sufficient to determine the center-of-mass motion of two-level atoms in an electromagnetic field, but they do not provide any information about the actual

phase-space distribution of the atoms. This can in some cases lead to wrong conclusions about the properties of the light forces. For example, it is seen from the Bloch equations that the dipole force vanishes on exact resonance. However, a more detailed analysis shows that a gradient force is exerted on the atoms even in this case. In contrast to the normal dipole force, this force is bidirectional and will split the wave function of a localized atom into two components that experience equal but oppositely directed forces. Since this leaves the center-of-mass motion of the atom unaffected, the splitting of the matter wave cannot be seen when applying the above analysis. Therefore, it is obvious that more rigorous methods are needed in the analysis of atom-optical elements based on the wave nature of atoms.

To determine the atomic phase-space distribution it is convenient to expand the total atomic wave function in the basis of the internal eigenstates as follows

$$\Phi(\vec{R},\vec{r},t) = \Phi_g(\vec{R},t)\phi_g(\vec{r})e^{-iE_gt/\hbar} + \Phi_e(\vec{R},t)\phi_e(\vec{r})e^{-iE_et/\hbar}, \tag{16}$$

where E_g and E_e are the ground and excited state energies, respectively. The equations of motion of the center-of-mass wave functions $\Phi_g(\vec{R},t)$ and $\Phi_e(\vec{R},t)$ can now be derived by substituting the above expansion into the Schrödinger equation and noting the orthogonality of the internal eigenstates. The resulting equations are, however, unsuitable for cases involving external relaxation processes. Furthermore, the interaction terms oscillate at optical frequencies, which is inconvenient in view of numerical calculations. These problems can be avoided by using the density matrix formalism, which finally gives the following equations for the combined evolution of the internal and external atomic dynamics [49]

$$\left(\frac{\partial}{\partial t} - \frac{\mathrm{i}\hbar}{M}\frac{\partial^2}{\partial\vec{R}\partial\vec{u}}\right)\sigma_{gg} = -\mathrm{i}\left[\kappa^*(\vec{R}+\frac{1}{2}\vec{u})\sigma_{eg} - \kappa(\vec{R}-\frac{1}{2}\vec{u})\sigma_{ge}\right], \tag{17a}$$

$$\left(\frac{\partial}{\partial t} - \frac{i\hbar}{M}\frac{\partial^2}{\partial\vec{R}\partial\vec{u}}\right)\sigma_{ee} = -\mathrm{i}\left[\kappa(\vec{R}+\frac{1}{2}\vec{u})\sigma_{ge} - \kappa^*(\vec{R}-\frac{1}{2}\vec{u})\sigma_{eg}\right], \tag{17b}$$

$$\left(\frac{\partial}{\partial t} - \frac{i\hbar}{M}\frac{\partial^2}{\partial\vec{R}\partial\vec{u}}\right)\sigma_{ge} = -\mathrm{i}\left[-\Delta\sigma_{ge} + \kappa^*(\vec{R}+\frac{1}{2}\vec{u})\sigma_{ee} - \kappa^*(\vec{R}-\frac{1}{2}\vec{u})\sigma_{gg}\right], \tag{17c}$$

$$\left(\frac{\partial}{\partial t} - \frac{i\hbar}{M}\frac{\partial^2}{\partial\vec{R}\partial\vec{u}}\right)\sigma_{eg} = -\mathrm{i}\left[\Delta\sigma_{eg} + \kappa(\vec{R}+\frac{1}{2}\vec{u})\sigma_{gg} - \kappa(\vec{R}-\frac{1}{2}\vec{u})\sigma_{ee}\right], \tag{17d}$$

where σ_{ij} are the elements of the density matrix $\rho_{ij}(\vec{R}+\frac{1}{2}\vec{u},\vec{R}-\frac{1}{2}\vec{u})$ in the position representation of the center-of-mass motion. Here the Rabi frequency is defined as $\kappa = \Omega(\vec{R},t)\exp(-\mathrm{i}\theta(\vec{R},t))/2$, and $\vec{u}$ describes the off-diagonality of the density matrix related to the spread of the atomic wave packet [50]. External relaxation processes may be included relatively easily into the above equations, as will be seen in the later sections.

Although Eqs. (17) include the internal and external evolution of the atomic wave function, they do not directly yield the phase-space distribution of the atoms. For that

purpose the equations have to be Fourier transformed with respect to $\vec{u}$ to give the equations of motion for the atomic Wigner function [51]

$$f(\vec{R},\vec{p}) = \frac{1}{(2\pi\hbar)^3}\int \Phi(\vec{R}+\frac{1}{2}\vec{u})\Phi^*(\vec{R}-\frac{1}{2}\vec{u})e^{-i\vec{p}\cdot\vec{u}/\hbar}\mathrm{d}\vec{u}. \tag{18}$$

From the definition of the Wigner function it is seen that the expectation value of an observable $\hat{\mathrm{A}}$, that depends either on $\vec{R}$ or $\vec{p}$, can be represented as $<A>=\int f\hat{\mathrm{A}}$. The Wigner function can, thus, be considered as a density function of the atom, even though it can in some cases have negative values. The distribution of the atom in, e.g., momentum space can now be calculated by integrating the Wigner function over the position coordinate. Another interesting property of the Wigner function is that it allows for a relatively simple analogy with the localized atoms. Namely, by assuming the phase-space distributions to be smooth on the scale $\hbar k$ and by calculating the expectation value over an assumedly localized center-of-mass position, the equations of motion for the Wigner function reduce to the equations (14).

3 Diffraction of Atoms by a Pulsed Standing Wave

Already in the 17th century it was noted that light deviates from its rectilinear propagation when it advances beyond a sharp obstruction. This phenomenon of diffraction, which stems from the wave nature of light, occurs also in the propagation of matter waves of particles with mass. Indeed, the beginning of atom optics can be traced back to the late 1920's when Estermann and Stern observed how a beam of neutral atoms was diffracted to several diffraction orders when it was scattered from the surface of a single crystal [2, 3]. In this case, the diffraction is due to the periodic ordering of the surface atoms that gives rise to a spatially varying modulation of the matter waves. In classical optics such periodic structures have been know as diffraction gratings already from the late 18th century, and they have been utilized extensively in spectroscopical applications. More recently, miniaturized grating structures have evolved into an important tool of modern optics by offering an efficient way to realize components for shaping and splitting wave fronts.

In the context of atom optics the use of diffractive elements has, traditionally, been hindered by the lack of high intensity atomic beams and the short de Broglie wavelength of atoms. For example, in atom interferometry the magnitude of the splitting angle of the matter waves can have a significant effect not only on the compactness of the experiment, but also on its sensitivity. Therefore, elements with a large diffraction angle are often preferred or are even required for a practical implementation of diffractive atom optics. Such elements have appeared only after advances in the theoretical and experimental understanding of the light forces and in nanofabrication techniques have been made. For example, nanofabricated structures with feature sizes of a few hundreds of nanometers have been applied to focus atomic beams [52], to split matter waves in interferometric applications [34, 35, 53], and they have even been used as computer generated holograms for matter waves [54].

The use of light forces for splitting and diffracting matter waves was suggested already in the late 1960's and 70's [11, 55–57]. The most common method is to use a standing wave as a light grating for neutral atoms. In this case, the diffraction is due to stimulated absorption-emission processes that lead to transfer of momentum from the optical field to the atom in discrete steps of $2\hbar k$. Complementarily, the process can be viewed as diffraction of matter waves from a phase grating of periodicity $\lambda/2$, which gives the same spacing for the diffraction angles. At optical frequencies, the period of the standing-wave pattern is on the order of a few hundreds of nanometers. Therefore, the angular separation of the diffraction orders, which is given by the ratio of the de Broglie wavelength λ_{dB} to the grating period, is limited to a few tens of μrads for thermal atoms. This is of the same order of magnitude as the diffraction angles obtained with nanofabricated transmission gratings. However, standing waves have the advantage of being able to produce large splitting angles even if the grating period is much larger than the wavelength of the matter waves. This is due to the fact

that the diffraction amplitudes of the high diffraction orders can be much higher than those achieved with normal transmission gratings.

An efficient use of the standing-wave grating requires that the atoms interact coherently with the light field. If external relaxation is significant during the interaction time, the coherence of the deflection will be reduced and the resulting momentum distribution of the diffracted atoms will contain a diffusive element. This has been shown both theoretically and experimentally for relaxation in the form of spontaneous emission [12, 49, 58–65]. The results of these studies show that if the number of spontaneously emitted photons is small during the interaction time, the momentum distribution of the diffracted atoms will consist of a double-peaked structure. The separation between the maxima in the angular distribution of the diffracted atoms is determined by the number of stimulated absorption-emission processes taking place during the interaction time.

The diffractive regime in the deflection of atoms can be achieved by tightly focusing two counter-propagating CW laser beams to form a narrow standing wave in the waist region [62, 63]. The interaction time for fast atoms crossing the standing wave can then be shorter than the spontaneous lifetime of the excited state. Another possibility to obtain a short interaction time is to use a pulsed laser as the light source [59, 66]. In this case, the interaction time may be limited by the pulse duration, which can be shorter than the spontaneous lifetime. An advantage of the pulsed laser scheme is that the intensity of the laser field can be several orders of magnitude higher than with CW lasers. This allows large splitting angles even for particles with a weak interaction with the field. It is typical for pulsed laser sources, however, that the coherence time of the light field is shorter than the interaction time. The coherence of the deflection will thus be influenced by the phase fluctuations of the laser field. In this thesis we are interested in the effects caused by the limited coherence of the laser field on the momentum distribution of the diffracted atoms. In the following, we first briefly describe the main concepts related to light gratings and then introduce a simple method to numerically determine the effects of the phase fluctuations [Paper I]. Finally, we compare the results with experimental measurements made for a thermal beam of sodium atoms [Paper II].

3.1 Light grating for neutral atoms

When dealing with diffractive atom optics, it is convenient to start by considering the motion of atoms in a time-independent potential $U_0(\vec{R})$. At low atomic velocities the internal atomic dynamics will follow adiabatically the changes in the external potential. In this case, the evolution of the center-of-mass wave packet $\Phi(\vec{R})$ can be calculated by solving the scalar Schrödinger equation, which according to the textbook

quantum mechanics takes the simple form

$$\left[\nabla^2 + K^2(\vec{R})\right] \Phi(\vec{R}) = 0, \tag{19}$$

where

$$K(\vec{R}) = \sqrt{2M[E - U_0(\vec{R})]/\hbar^2} = n_r(\vec{R})K_0 \tag{20}$$

is the wave number of the matter wave, $K_0 = \sqrt{2ME/\hbar^2}$, and E is the energy of the atom. Equation (19), which closely resembles the Helmholtz equation of classical optics, describes the motion of matter waves in a "medium" of refractive index $n_r(\vec{R})$. This similarity in the evolution of electromagnetic and matter waves justifies the name *atom optics* for applications relying on the wave nature of atoms. The biggest difference between classical and atom optics is due to the finite mass of atoms, which yields a mass-dependent dispersion relation for matter waves.

Since the evolution of the atomic wave function is described by an equation analogous to the Helmholtz equation, the methods known from classical optics are suited also for the analysis of matter wave diffraction. In fact, the diffraction integrals formulated by Kirchhoff are even more suitable for atomic matter waves than for electromagnetic waves. This is due to the small wavelength of the matter waves, as compared with the typical feature size of the diffractive elements used to control the atomic motion. Also, atoms are usually adsorbed on or diffusively scattered by surfaces, and thus the assumption of vanishing wave function at the boundary is nicely satisfied. Following the formalism of classical optics, the diffracted matter wave can be deduced from

$$\Phi(\vec{R}) = -\frac{iK_0}{2\pi} \int \Phi(\vec{R}_0) \frac{\vec{n} \cdot \vec{R}}{|\vec{R} - \vec{R}_0|^2} \left(1 + \frac{i}{k_0|\vec{R} - \vec{R}_0|}\right) e^{iK_0|\vec{R}-\vec{R}_0|} \, \mathrm{d}R_{0x}\mathrm{d}R_{0y}, \tag{21}$$

where $\Phi(\vec{R}_0)$ denotes the wave function on the object plane. This is just the Rayleigh-Sommerfeld formulation of the Huygens' principle, and gives the diffracted wave as a sum of the elementary waves emitted from each point on the object plane. Obviously, Eq. (21) will reduce to the familiar Fresnel and Fraunhofer expressions in the limit of near- and far-field diffraction, respectively.

Let us next consider the diffraction of atoms from a standing wave. The position distribution of the atoms at a given distance from the object plane can be calculated by solving the diffraction integral, Eq. (21), with a suitable object plane wave function. Since we are dealing with a light grating, this function has to be determined from the time-dependent Schrödinger equation for the total atomic wave function. Here we assume that the internal atomic motion can be neglected, and we describe the effects of the standing wave on the center-of-mass motion of the atoms with a scalar potential given by

$$U(x) = U_0 \cos^2(kx), \tag{22}$$

where k is the wavenumber of the light field. In this case, the equation of motion for the atomic wave function reduces to the scalar Schrödinger equation with the scalar

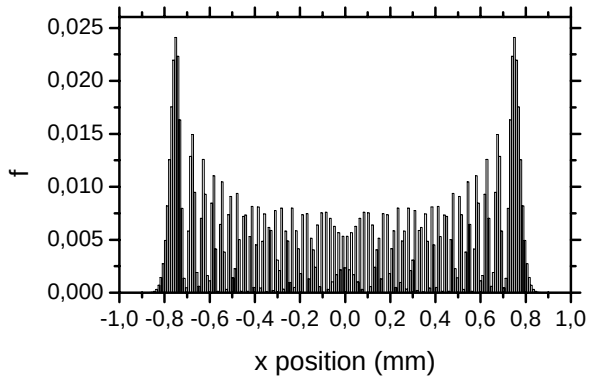

Figure 4: Position distribution of sodium atoms diffracted by a standing wave of wavelength 589 nm. The distribution corresponds to an interaction time of 10 ns and a potential depth of 11 meV. The distance from the object plane is 50 cm and the atomic beam velocity is 500 m/s. The fraction of atoms in a specific position on the observation plane is given as f on the vertical axis.

potential (22) describing the interaction. At short interaction times the light field does not have a significant effect on the position distribution of the atoms. In this case, the standing wave acts as a pure phase grating, and the atomic wave function after the interaction with the light field over the time T takes on the simple form

$$\Phi(\vec{R}_0) = \Phi_{\rm i}(\vec{R}_0) e^{-i\frac{[E-U(x)]T}{\hbar}}, \tag{23}$$

where $\Phi_{\rm i}(\vec{R}_0)$ is the initial state of the atom. This corresponds to the familiar Raman-Nath approximation, which requires that the atoms do not move considerably in the direction parallel to the laser beams during the interaction time. The diffracted matter wave at a given distance from the standing wave can now be calculated by substituting the above expression to the diffraction integral. In the far field, i.e., within Fraunhofer approximation, the diffraction integral reduces to the Fourier transformation, which gives the atomic distribution as

$$|\Phi(x,L)|^2 = \sum_{n=-\infty}^{\infty} J_n^2\left(\frac{U_0 T}{2\hbar}\right) \delta(x - 2nLk/K_0), \tag{24}$$

where L is the distance from the object plane and J_n is the Bessel function of nth order. Here we have also assumed that the initial state is spread out to a region much wider than the wavelength of the light field. Equation (24) shows that the atoms are diffracted into discrete angles given by the grating equation $\Theta_d = \lambda_{dB}/d$, where $d = \lambda/2$ is the grating period. The fraction of atoms diffracted to the n*th* diffraction order is given by $J_n^2(U_0 T/2\hbar)$. For example, Fig. 4 shows the position distribution of a monoenergetic sodium atom beam diffracted by a standing wave of wavelength 589 nm.

The phase-grating analogy for the standing wave applies only when the atoms stay in some well-defined state that adiabatically follows the changes in the optical field throughout the interaction. Furthermore, it neglects the effects of the photon recoil on the atomic distributions and requires that the coherence of the matter wave is not lost in the interaction. In a more general case, i.e., when non-adiabatic transitions between the different internal states or external relaxation processes cannot be neglected, the wave function description of the atoms becomes unsuited for the calculations and a more general approach must be adopted. A suitable choice for such a case is to use the density matrix description for the atoms, which can take into account the statistical mixtures of the states (another possibility is to use the Monte Carlo wave function approach [67]). For two-level atoms the density matrix equations that include both the internal and external evolution of the atoms are given in Eqs. (17) (without the relaxation terms).

The diffraction profile of the atoms can now be calculated by solving the diagonal components of the atomic density matrix at a given time and by taking a Fourier transformation with respect to the variable $\vec{u}$, as discussed in Sec. 2 of this overview. This will give an expression for the Wigner function of the atoms, which includes the information about the atomic distribution in both position and momentum spaces. Within the Raman-Nath approximation and assuming that the interaction terms are constant in time, the Wigner function can be calculated analytically [49]. In this case, the momentum distribution of the atoms after the interaction with a resonantly tuned standing wave is given by [11, 68–70]

$$\mathcal{P}(p) = \sum_{n=-\infty}^{\infty} J_n^2 \left(\frac{1}{2}\Omega_0 T\right) \delta(p - n\hbar k), \tag{25}$$

where p is the momentum in the direction of the laser beam and Ω_0 is the Rabi frequency corresponding to the amplitude of the standing wave. The above expression shows that the atoms are diffracted into discrete angles and that the fractional amplitude of the different orders follows the Bessel-function distribution. However, compared with the distribution given in Eq. (24) the diffraction angles are now halved.

As can be seen from Eq. (25), the rate of momentum transfer from the optical field to the atoms is proportional to the Rabi flipping frequency. For laser fields with a finite spectral width, the coherence of the atom diffraction will thus depend on the ratios of the Rabi period to the coherence time $\tau_{\rm c}$ of the field and to the interaction time T. If the coherence time is much shorter than the Rabi period and the interaction time, i.e., $\tau_c \ll \Omega^{-1}, T$, the atoms will be deflected diffusively and their final momentum distribution will have a Gaussian shape [69, 70]. In the other extreme, for $\tau_c = \infty$, the deflection will be fully coherent and the resulting momentum distribution can be described using the diffraction analysis. In this case, the shape of the momentum distribution depends on the experimental conditions and can be described as being due to either the Kapitza-Dirac process [62,63] (see Eq. (25)), the Stern-Gerlach effect [71]

or the Bragg scattering [72]. For pulsed lasers, the coherence time will typically be in between the above regimes, and the momentum distribution will include both a diffractive and a diffusive component. This intermediate regime of the coherence time constitutes a main subject of this thesis.

3.2 Diffraction of atoms by a pulsed standing wave

In general, the diffraction of atoms from a fluctuating standing wave is a complicated problem, and the results depend on the details of the coherence properties of the light field [73]. The fluctuating parameter can be either phase, frequency, amplitude, or even all of them at the same time. Depending on the experimental conditions, various models can be applied to describe the random variable, with differing results and degrees of theoretical complexity. For example, the phase of the laser field can change diffusively in time (the so called phase-diffusion model, see, e.g., [74–77]); or it may undergo random jumps at random time intervals (the random-jump model, see, e.g., [78–80]).

In addition to the specific noise process, the momentum distribution of the diffracted atoms depends on the correlation between the phases of the two counter-propagating laser beams forming the standing wave. If the phases of the laser beams are independent, both the node positions and the phase of the standing wave will fluctuate in time. For optical fields with a large bandwidth, i.e., $\delta\omega \gg \Omega$, the deflection can then be described with the random-walk model, and the final momentum distribution will show a diffusive character. In contrast, if the phases of the counter-propagating laser beams are identical, the node positions are fixed and only the phase of the standing wave fluctuates. Obviously, this case corresponds to a standing wave formed, e.g., by folding a laser beam back onto itself by a mirror and restricting the interaction region to a distance smaller than the coherence length. Since the intensity distribution of the field is inhomogeneous, the final momentum distribution will not be strictly Gaussian even at large bandwidths. From a practical point of view, most of the diffraction experiments are done in the latter configuration, i.e., when the node positions are fixed. It is, therefore, interesting to study the effects of the phase fluctuations on the final momentum distributions in this geometry (see Fig. 5).

For pulsed lasers oscillating in several longitudinal modes, a complete analytical description of the stochastic noise processes would lead to very complicated equations for the atomic variables, which would be laborious to solve even numerically. Therefore, computer simulations based on Monte-Carlo methods are often used to determine the atomic response to pulsed laser fields. The results of such calculations might not, however, be very instructive in describing the general properties of the diffraction process. To avoid such problems, we adopt a simple approach to the stochastic processes and use the phase-diffusion model to describe the effects of the finite bandwidth of the laser field to the coherence of the diffraction. Although this model does not fully

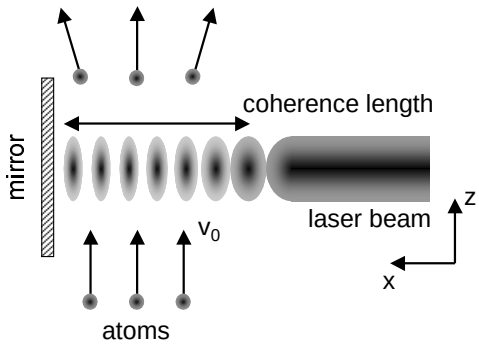

Figure 5: Geometry of the standing-wave grating for atoms considered in this thesis.

describe pulsed laser behavior, it clearly illustrates the role of the coherence time on the diffraction process. Moreover, it leads to a numerically convenient expression for the final momentum distribution.

Assuming that the phase-diffusion is driven by a δ-function correlated Gaussian random process and that the laser field has a Lorentzian spectrum with a width of $\delta\omega$ (FWHM), the equation of motion for the ensamble averaged density matrix can be written as in Eqs. (17), but with a relaxation term $-\Gamma\sigma_{ab} = -\delta\omega\sigma_{ab}/2$ included in the off-diagonal terms [81]. The momentum distribution of the atoms can now be calculated in the same way as was done in the previous subsection. We first take the Laplace transform of the density matrix equations and solve the impulse-response function for the diagonal terms [Paper I]

$$I(x,u,T) = e^{-\frac{1}{2}\Gamma T}\left[\cos(\omega_1 T) + \frac{\Gamma}{2\omega_1}\sin(\omega_1 T)\right], \tag{26}$$

where $\omega_1 = \sqrt{K^2 - (\Gamma/2)^2}$ and $K(x,u) = \Omega_0 \sin(kx)\sin(\frac{1}{2}ku)$. We proceed by using the impulse response to propagate the initial state through the interaction time and take the Fourier transformation of the result with respect to the variable u. This yields an expression for the atomic Wigner function, which after integration over the position space gives the final momentum distribution of the atoms. Assuming that the initial state of the atomic beam is spread in position space over many wavelengths and taking into account the periodicity of the standing-wave pattern, the final momentum distribution can be calculated from

$$\mathcal{P}_f(p,T) = \sum_{n=-\infty}^{\infty} P_n(T)\delta(p - n\hbar k), \tag{27}$$

where

$$P_n(T) = \frac{1}{\lambda^2}\int_{-\lambda/2}^{\lambda/2}\int_{-\lambda/2}^{\lambda/2} I(x,u,T)e^{-inku}\mathrm{d}u\mathrm{d}x, \tag{28}$$

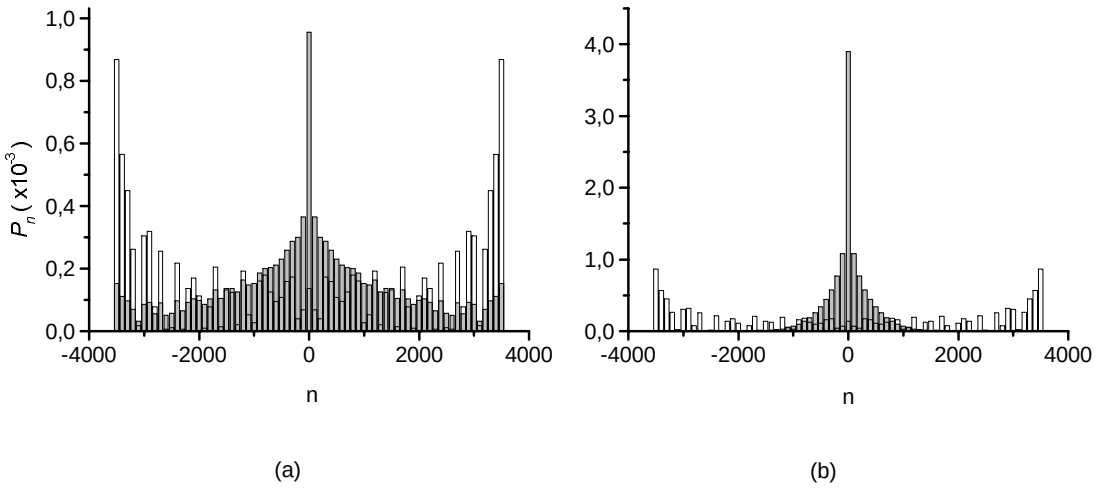

Figure 6: Calculated momentum distributions for sodium atoms after interaction with a pulsed standing wave of high field intensity for two values of the laser bandwidth. The interaction time and the Rabi frequency are $T = 7\,\text{ns}$ and $\Omega_0 = 1 \times 10^{12}\,\text{s}^{-1}$, respectively. In (a) $\delta\omega = 0.94 \times 10^9\,\text{s}^{-1}$ and in (b) $\delta\omega = 18.8 \times 10^9\,\text{s}^{-1}$. The probabilities for observing atoms in the momentum states $n\hbar k$ are represented by the filled bars. The unfilled bars correspond to the momentum distributions with zero relaxation.

and λ is the wavelength of the light field. The coefficients $P_n(T)$ can be interpreted as probabilities of the atoms to end up in the final momentum state $n\hbar k$.

From Eq. (26) we can see that the phase fluctuations of the laser field cause the impulse response to decay exponentially. In the limit $\Gamma = 0$ the impulse response reduces to that of coherent diffraction, and the final momentum distribution is given by Eq. (25). For fast relaxation, i.e. $K/\Gamma \ll 1$, the laser field loses its coherence on a time scale of the Rabi period. In this case, the impulse response is given by the rate-equation approximation [16, 81], and the deflection profile will have a diffusive character [70]. In the intermediate region, the deflection profile has both a diffractive and a diffusive component, and has to be calculated using Eqs. (26)–(28).

Fig. 6 shows the final momentum distribution of atoms diffracted from a pulsed standing wave for two values of the laser bandwidth [Paper I]. The two profiles correspond to a narrowband and a broadband operation of a typical pulsed dye laser with a bandwidth of $\delta\nu = 0.15\,\text{GHz}$ and 3 GHz, respectively. In both cases, the Rabi period is much shorter than the coherence time of the field, and thus some coherent effects are expected to be seen. For the case of the narrowband operation [Fig. 6(a)], the coherence time is long enough so that on the average only a few phase jumps will occur during the interaction time. The effect of these phase jumps can be seen in the calculated momentum distribution as a transfer of atoms mostly to the low momentum

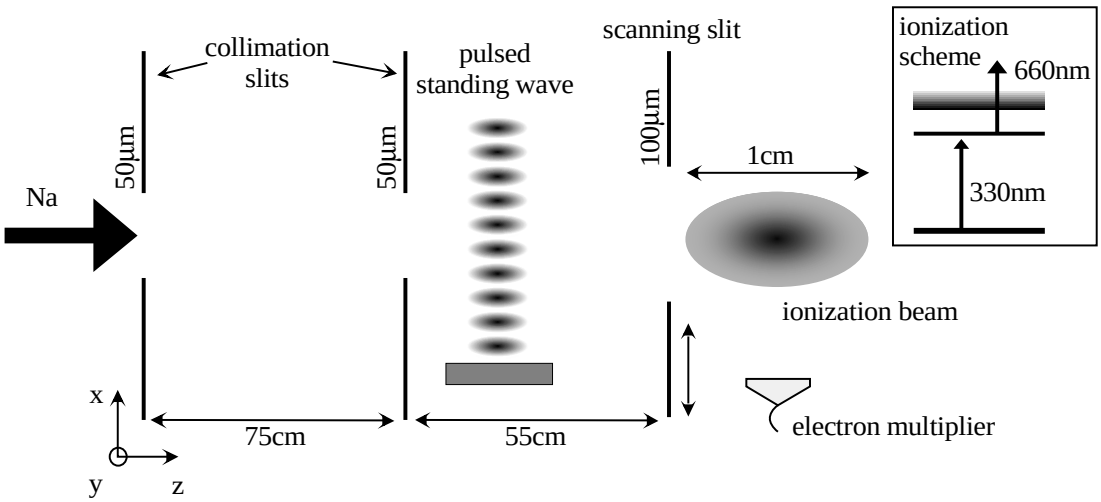

Figure 7: Experimental setup for measuring the deflection profile of a sodium beam by a pulsed standing wave.

states. If the coherence time is decreased, the number of atoms in the two side maxima will be significantly reduced. For the bandwidth value of Fig. 6(b) the momentum distribution is already mainly diffusive.

To compare the theoretical results with experiments we have performed diffraction measurements for a thermal beam of sodium atoms interacting with a pulsed standing wave [Paper II]. The experimental setup used in the measurements is depicted in Fig. 7. The atomic beam, produced by thermal evaporation of metallic sodium, is collimated using two narrow slits with dimensions 50μm$\times$ 1 cm positioned 75 cm apart. The standing wave was produced by retro-reflecting a collimated laser beam from a flat dielectric mirror. The laser source was a pulsed Nd:YAG laser pumped dye laser (Quantel YG580 and TDL50). The transverse spatial profile of the laser beam was elongated with an approximately Gaussian intensity profile in the z-direction and a constant intensity across the atomic beam in the y-direction. The smoothness of the intensity distribution across the laser beam was improved by spatial filtering.

The atomic beam profile after the deflection was measured using a 100 μm$\times$1 cm scanning slit together with ion detection. The slit was positioned 53 cm downstream from the interaction region. Atoms that passed through the slit were optically ionized in a two-step process (see Fig. 7) using an excimer laser pumped pulsed dye laser (Lambda Physik EMG 103 and FL2002) with a pulse duration of about 10 ns as the radiation source. Finally, the photo ions were accelerated to 2500 eV and detected with an electron multiplier. Advantages of this detection method include the high sensitivity of the ionization scheme to only the selected atomic species, and the possibility for a good time-of-flight resolution. In our case the velocity resolution in the z-direction was about 20 m/s, determined by the 1 cm width of the ionizing laser beam.

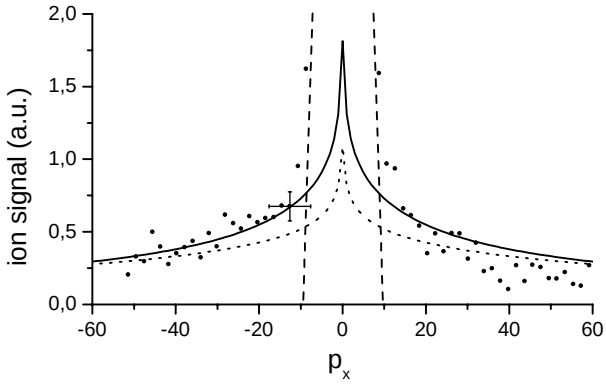

Figure 8: Momentum distribution of sodium atoms deflected by a pulsed standing wave. The transverse momentum p_x is given in units of $\hbar k$. The experimental data are represented by dots. The dotted line is a theoretical momentum distribution based on Eq. (27) using the upper-limit value of $\Omega = 1.78 \times 10^{12}\,\mathrm{s}^{-1}$ for the effective Rabi frequency. The solid line represents the theoretical momentum distribution with the Rabi frequency and the coherence time reduced by a factor of two. The experimental error bars are indicated for one data point. The dashed line is the profile of the atomic beam without the deflecting laser pulses.

Fig. 8 shows a comparison between the experimental and theoretical momentum distributions for the sodium atoms after interaction with a resonantly tuned pulsed standing wave with a duration of 9 ns (FWHM). The measurement corresponds to an intermediate value of the coherence time, i.e. $T > \tau > \Omega^{-1}$, measured to be ~ 0.1 ns. An estimated upper-limit value for the effective Rabi frequency at the peak of the Gaussian spatial distribution was $\Omega = 1.78 \times 10^{12}\,\mathrm{s}^{-1}$ (calculated using the line strength $S = 25.4\, a_o^2 e^2$ for the sodium D_2 line [82]). The measured momentum distribution is illustrated with dots in Fig. 8 and the corresponding theoretical distribution, including the effects of the Gaussian intensity profile of the laser beam in the z-direction, is shown with the dotted line.

Since the thermal atomic beam is continuously on, there will always be a large amount of atoms in the detection zone that were not in the interaction zone at the time of the standing-wave pulse. Therefore, the measured distribution is dominated at the low momentum values ($|p_x| \leq 10\hbar k$) by these non-deflected background atoms, and our measurement will only reveal the higher-momentum part of the diffracted distribution. The main characteristics of the deflection profile are, however, visible from the data at the high-momentum states. The experimental transverse momentum resolution was limited to $10\,\hbar k$ mainly by the width of the scanning slit, the divergence of the atomic beam, and its width at the position of the standing wave. The effects of the measurement resolution on the observed distribution are small for the high-momentum states, and were therefore neglected.

We notice that the theoretical momentum distribution (the dotted curve) is spread out more than the experimental distribution. This is as expected, since the momentum distribution is quite sensitive to the value of the Rabi frequency, which for the dotted curve was calculated by assuming that all laser modes are resonant with the atomic transition. If the hyperfine structure of the transition and the mode structure of the laser were taken into account, the effective Rabi frequency would be reduced from the estimated upper-limit value. Also, due to the multimode structure of the diffracting laser beam, the exact value of the coherence time τ_c probably differs from the inverse of the laser bandwidth. As shown by the solid line in Fig. 8, a factor of two reduction of the stated values of the Rabi frequency and the coherence time already brings about a much better fit between the experimental data and the theory.

4 Pulsed Mirrors for Neutral Atoms and Molecules

In analogy to classical optics, mirrors that efficiently reflect matter waves play a major role in applications of atom optics. Atom mirrors can be used, for example, to steer and image atomic beams, to guide and confine atoms in selected spatial regions or even to decelerate atomic beams by inelastic reflections. The large variety of possible applications has been one of the driving forces in the pursuit to develop efficient atom mirror configurations throughout the history of quantum mechanics. Indeed, the first atom mirror appeared already in 1929, when Knauer and Stern reflected a beam of He atoms with the aid of crystal surfaces [83]. However, it required the development of tunable lasers and improved understanding of the light forces until mirrors suitable for atom optics could be developed. In view of atom optical applications, the surface reflection is unattractive due to its inherently diffusive character. Furthermore, the attractive van der Walls forces result in large sticking probabilities of atoms to the cooled surfaces, which can limit the reflection efficiency to impractically low values. In contrast, atom-photon interactions are relatively simple and can be controlled accurately by varying the laser parameters. With suitable parameter values reflection efficiencies close to 100 % can be achieved, which makes mirrors based on light forces ideal for applications of matter-wave optics.

Typically, atom mirrors rely on the dipole force exerted on the particles by inhomogeneously distributed optical fields, which are tuned close to a suitable atomic resonance frequency. In the case of blue detuning, the dipole force is repulsive and the optical field acts as a potential barrier for neutral atoms. In analogy to classical optics, elastic reflection can then be obtained at angles of incidence smaller than the critical angle for total internal reflection. Various field configurations based on, e.g., the use of evanescent waves [84–86] and the doughnut mode optical fields [87] have been applied to generate the repulsive potential for atomic species. In addition to the total internal reflection, light forces can be utilized also as quantum reflectors for matter waves. The simplest reflector of this type is a potential step, which, according to textbook quantum mechanics, can be utilized as a partial reflector in analogy to a single dielectric surface in classical optics. This type of reflection has been analyzed, e.g., for a red-detuned evanescent wave that acts as an attractive exponential potential [88]. An obvious generalization of the single-step quantum reflection is to apply a periodic potential as a "dielectric" mirror for matter waves. At suitable incident kinetic energies, the partial reflections at successive potential steps will interfere constructively and allow a high reflection coefficient to be obtained [72, 89–92]. Currently, atom mirrors that are based on light forces are used in various applications of atom optics, e.g., in confining neutral atoms into gravitational cavities [87, 93], as atomic wave guides [94, 95] or as mirrors in atom interferometers [96].

A common feature of the above atom mirrors is the use of CW lasers as the light source. Due to the relatively low field intensities available from the wavelength-tunable CW

lasers, the reflectivity of the atom mirrors rapidly decreases for atomic velocities on the order of a meter per second or higher. This velocity limit may be increased somewhat by applying field enhancement techniques based on, e.g., the surface plasmon effect or on the use of optical build-up cavities [97–100]. These techniques are, however, far too ineffective for the reflection of atoms with velocities in the thermal range. The use of the conventional atom mirrors is then limited to grazing incidence reflection of atomic beams or to the control of initially laser cooled atoms. Moreover, since the magnitude of the light forces at low field intensities is very sensitive to the internal energy-level structure of the atom, the use of the conventional atom mirrors is also limited to the reflection of some particular atom species only.

In this thesis, we introduce a novel type of pulsed atom mirror that extends the conventional methods towards reflection of higher initial velocities and reflection of more complex particles. When using a pulsed laser as the light source, the field intensity can be increased by several orders of magnitude compared to the case of a typical CW laser. Then the dipole forces can become strong enough to significantly affect the atomic motion up to velocities of several tens of meters per second. This allows large-angle reflection of atomic beams, or even reflection of thermal atoms at normal incidence. Also, in the case of pulsed fields the dipole forces experienced by the particles remain strong even at large detunings from the atomic resonance. Pulsed atom mirrors will, therefore, be much less sensitive to the internal energy-level structure of the atom. Consequently, atom optical components based on pulsed laser fields are attractive also for the manipulation of multilevel atoms and even molecules [101–105].

4.1 Pulsed evanescent-wave mirror

The use of evanescent waves for the reflection of neutral atoms was proposed already in 1982 by Cook and Hill [84] (see Fig. 9). Since then the evanescent-wave mirror has become one of the most widely studied components of atom optics. The studies have demonstrated the value of the evanescent-wave mirror not only as an elastic reflector [85, 86, 106], but also as a reflection grating for matter waves [107–110]. Furthermore, evanescent waves have been incorporated to atom interferometry [96, 111], and they have been used to guide atoms through hollow-core optical fibers [112, 113] as well as to trap [93, 114, 115] and cool neutral atoms [116–121]. Today, the evanescent-wave mirror has become a standard tool in atom optics with a broad range of applications in controlling the motion of slow atoms.

In this thesis, we study the application of strong-field laser pulses of a few nanoseconds duration to extend the usability of evanescent-wave mirrors to higher incident atomic velocities. When relying on the dipole force as the reflection mechanism, the depth of the optical potential at an optimal value of the detuning is, typically, proportional to the maximum value of the Rabi frequency in the laser field. Therefore, the highest

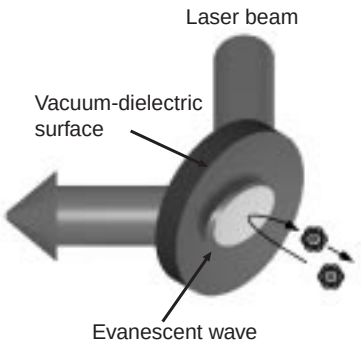

Figure 9: The evanescent-wave atom mirror.

incident velocity that can be reflected grows with intensity roughly as $\sim I^{1/4}$. This weak dependence on the intensity is the main reason why pulsed lasers are required if atoms significantly faster than those currently manipulated with CW lasers are to be reflected. For example, to increase the reflected velocity from 1 m/s to several tens of meters per second an increase in laser intensity of more than six orders of magnitude is required. Clearly, this will require the use of pulsed lasers (compare with the 100 fold increase in intensity obtainable with surface plasmons).

At high initial velocities of the atoms, the spread of the atomic wave packet is small compared with the decay length of the evanescent wave. In this case, the phase-space distribution of the atoms can be neglected in the calculation of the atomic dynamics. For two-level atoms the center-of-mass motion can then be determined by integrating the Bloch-Ehrenfest equations, Eqs. (14), over the interaction time. Since we are dealing with pulsed laser fields with a duration on the order of, or shorter than, the spontaneous lifetime of the excited state, the steady-state solution of the Bloch vector cannot be used to determine the light forces. In addition, the coherence time of the pulsed laser field is often shorter than the pulse duration and should, therefore, be considered in the calculations. These factors complicate the calculations and do not generally allow a closed-form solution for the light forces. For such cases the atomic motion should be determined by integrating Eqs. (14) numerically. This can, however, lead to a very long consumption of CPU time. To avoid such problems we make some simplifying assumptions that allow us to determine the atomic motion during the laser pulse with numerical integration required only for the center-of-mass motion.

To simplify the physical situation we assume that the amplitude of the laser field remains constant during the laser pulse. Furthermore, we apply the phase-diffusion model to describe the effects of the limited coherence time of the laser field on the Bloch vector behavior. This leads to a simple exponential decay of the coherence terms of the ensemble-averaged Bloch vector with a characteristic time given by the inverse of the spectral width $\delta\omega$ of the laser field [81]. To calculate the atomic motion, we first determine the Bloch vector for atoms at rest in the laser field and then use the

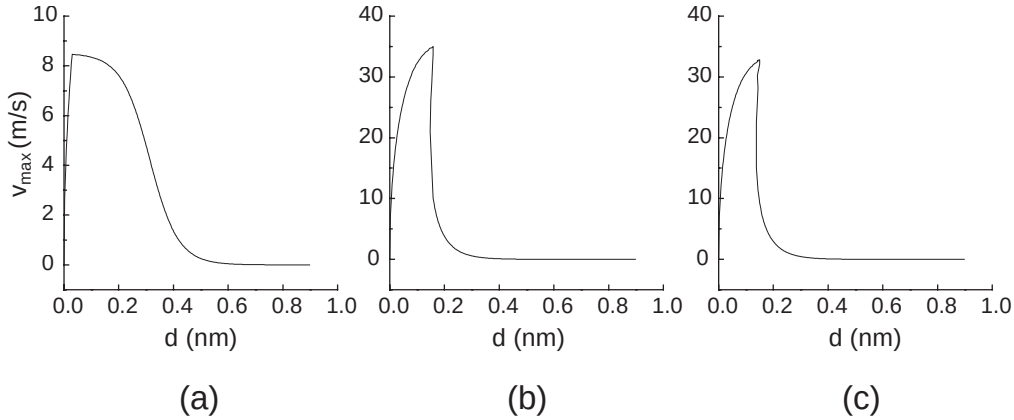

Figure 10: Maximum incident velocity v_{max} of sodium atoms reflected by a 10 MW/cm^2 evanescent wave, plotted as a function of the initial distance d of the atoms from the mirror surface for three different atom-field detunings. In (a) $\Delta = 0.1 \times 10^{12}\,\mathrm{s}^{-1}$, in (b) $\Delta = 1.6 \times 10^{12}\,\mathrm{s}^{-1}$, and in (c) $\Delta = 2.0 \times 10^{12}\,\mathrm{s}^{-1}$. The pulse duration is 7 ns, and the e^{-1} depth of the evanescent wave is 56 nm.

solution to approximate the evolution of the moving atoms [Paper III].

Since we are dealing with a pulsed laser field, the potential barrier height will be different for atoms that start at different locations at the turn-on time of the laser field. Therefore, the maximum reflected velocity will not be constant, as in the case of CW laser fields, but will change as a function of the distance from the dielectric surface. This is illustrated in Fig. 10 for sodium atoms moving in an evanescent wave with a maximum intensity of 10 MW/cm^2. In this case, atoms with initial velocities up to about 35 m/s can be reflected. This is on the same order of magnitude as can be estimated by using the $I^{1/4}$-dependence for the maximum reflected velocity. From Fig. 10 we can also see that the maximum reflected velocity decreases rapidly for atoms that start beyond the decay length of the evanescent wave. This limits the effective volume from which the atoms can be reflected to a relatively small value, which can be a severe problem when using lasers with a low repetition rate. The effective interaction volume can be increased either by using longer laser pulses or higher intensities.

Another important feature of the pulsed evanescent-wave mirror is that the atoms are not reflected elastically. This is due to the fact that the force exerted on the atoms varies as a function of the initial position. Therefore, for a finite pulse duration, at least some atoms will end up at having a final velocity different in magnitude from the initial velocity and thus the reflection will be inelastic. Although this is an undesirable effect in atom optical applications, it can be useful in controlling the motion of thermal atoms. This is illustrated in Fig. 11 for a thermal beam of sodium atoms normally incident on a pulsed evanescent wave with a maximum intensity of 10 MW/cm^2. Clearly,

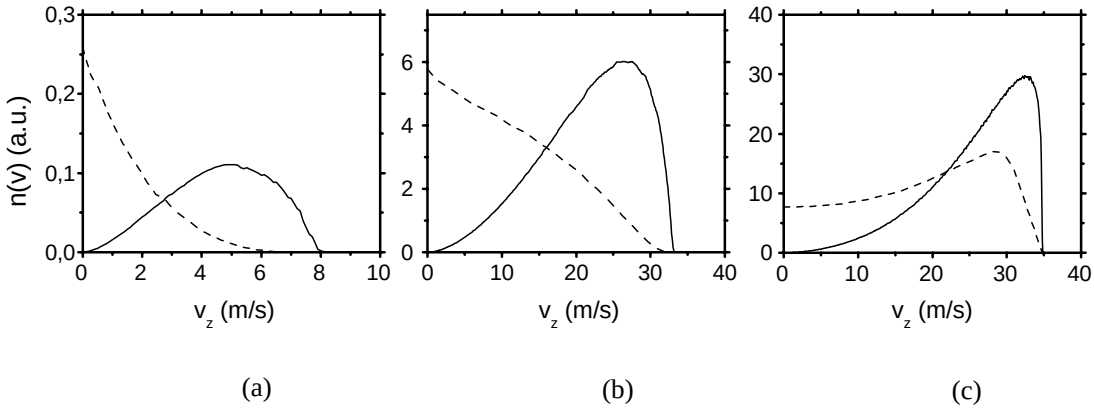

Figure 11: Modification of the thermal velocity distribution in reflection from an evanescent-wave mirror for three different pulse durations t_p; (a) $t_p = 1\,\mathrm{ns}$, (b) $t_p = 10\,\mathrm{ns}$, and (c) $t_p = 15\,\mathrm{ns}$. The incident velocity distribution of atoms undergoing reflection is indicated by the solid line, and the distribution after the reflection is indicated by the dashed line.

the velocity distribution of the reflected atoms can be modified by changing the interaction time. At short pulse durations the atoms do not have time to move through the whole evanescent wave and the reflection will be mostly inelastic. In this case, the atoms tend to be concentrated on the low velocities. For longer pulses, the interaction time is sufficient for a large part of the atoms entering the evanescent wave to undergo elastic reflection. The velocity distribution of the reflected atoms will thus approach their initial distribution when the pulse length is increased.

Compared with the conventional atom mirrors, the pulsed evanescent-wave mirror provides reflection angles that are larger by an order of magnitude. This is an important factor, especially, when dealing with thermal atomic beams, for which the CW mirrors are efficient only at grazing incidence. Furthermore, the velocity distribution of the reflected atoms can be modified by changing the pulse duration. In particular, at short pulse durations atoms reflected from a thermal beam tend to concentrate at low velocities. This type of reflection could be interesting for slowing down multilevel atoms, for which the usual Doppler-cooling methods are ineffective. For such a method to be practical, the number of reflected atoms per unit time should be as high as possible. At typical intensity levels, the effective volume from which the atoms can be reflected is, however, rather small (see Fig. 10). For normal incidence, this limits the number of reflected atoms in a typical thermal atomic beam to ca. 1000 atoms/s (at 10 Hz repetition rate) even if all atoms slower than 35 m/s would be reflected. Faster accumulation of atoms could be achieved by using a higher pulse repetition rate.

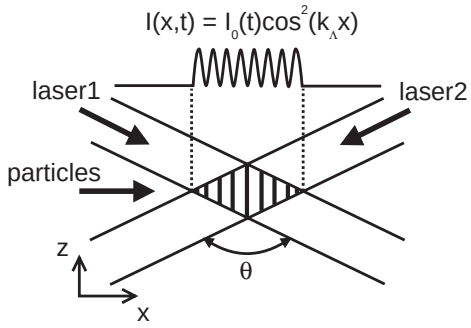

Figure 12: The geometry of the pulsed standing-wave mirror.

4.2 Pulsed standing-wave mirror

The conventional atom mirror configurations, including the pulsed evanescent-wave mirror, make use of a repulsive optical potential for the reflection of the atoms. As shown in Sec. 2, such potentials can be generated with the aid of dipole forces, but they require near-resonant light fields with a blue detuning. Unfortunately, this limits the use of the conventional atom mirrors to reflection of only simple atoms. For example, the rich internal energy-level structure in molecules makes it necessary to apply fields tuned sufficiently far below all electronic resonances to generate the dipole force. In this case of quasistatic fields, the dipole force exerted on ground state molecules will, unfortunately, always be attractive, i.e., towards the high-intensity regions of the optical field [122]. The motion of molecules through, e.g., a quasistatic evanescent wave is then analogous to the propagation of light through a medium with increasing refractive index, where total internal reflection is forbidden.

Possible solutions to the problem posed by the attractiveness of the potential are to excite the molecules to Rydberg levels, or to use a suitable quantum reflector. Although repulsive dipole forces can be obtained for Rydberg molecules [122], the need for high excitation severely limits the range of applications of such methods. Quantum reflectors, on the other hand, work with both repulsive and attractive forces, but are limited to very small incident velocities. In the following we introduce a novel scheme based on the use of a pulsed standing wave to reflect neutral particles that does not suffer from the above problems [Papers IV and V].

The geometry of the pulsed standing-wave mirror (PSWM) studied in this thesis is shown in Fig. 12. The main idea is to use each period of the standing-wave pattern as an independent mirror for the incoming particles. In the general case, the reflection will be inelastic, since the particles start at different locations at the turn-on time of the laser pulse. However, it is possible to obtain elastic reflection with a suitable choice of the field intensity and pulse duration [Papers IV and V]. To derive the optimum conditions for elastic reflection, we model the effects of the pulsed standing wave on

the center-of-mass motion of the particles with a position dependent effective potential. Furthermore, we apply the quasiclassical approximation in the calculation of the final momentum distribution of the particles. This is allowed, since the total momentum transferred to the atoms in a pulsed laser field is typically much larger than a single recoil momentum. In this case, we can neglect the $\hbar k$ scale features in the momentum distribution and use the classical equations of motion to describe the motion of the particles.

In the case of an attractive (repulsive) dipole force, particles that start within the interaction region are caught by the standing wave and start to oscillate around the antinode positions (node positions). If the effective potential depends linearly on the field intensity, the potential wells around the the antinodes will be nearly parabolic. This allows a harmonic-oscillator analysis to be applied to calculate the final velocity of the particles. For laser pulses with a square-shaped temporal profile the resulting expression for the final velocity takes the simple form

$$p_f = p_i \cos(\omega_{\rm osc} T) - M\omega_{\rm osc} x_i \sin(\omega_{\rm osc} T), \tag{29}$$

where $\omega_{\rm osc} = 2\pi/T_{\rm osc}$ is the oscillation frequency and x_i the initial x-coordinate value of the particle in the potential well. From the above equation we can clearly see that by choosing the interaction time such that

$$T = \left(n - \frac{1}{2}\right) T_{\rm osc} \quad (n = 1, 2, ...), \tag{30}$$

all particles will end up having final momenta $p_{\rm f} = -p_{\rm i}$, regardless of their velocities and positions in the well at the turn-on time of the laser field. With this choice of the oscillation period, the PSWM acts as a long row of independent atom mirrors. Due to the symmetry of the standing-wave pattern, elastic reflection can be obtained both with attractive and repulsive forces.

An additional advantage of the PSWM compared with, e.g., the pulsed evanescent-wave mirror is the possibility to obtain a large interaction volume without compromising the strength of the dipole force. Since each period of the standing-wave pattern provides the same dipole force to the particles, the PSWM can be used to control a large number of particles even with a single laser pulse. Moreover, the standing-wave geometry gives the strongest possible intensity gradient at a given wavelength, and thus provides the strongest possible forces, too. This is very convenient, especially, when dealing with off-resonant fields that otherwise can lead to relatively small potential depths.

The fraction of elastically reflected particles for the first reflection optimum ($n = 1$) is, typically, limited to roughly 20% due to the anharmonicity of the sinusoidal standing-wave potential [Paper V]. Furthermore, the anharmonicity leads to a rapid decrease of the reflection coefficient of the PSWM at initial velocities of $v_{\rm i} \gtrsim \Lambda/2T$, where Λ is

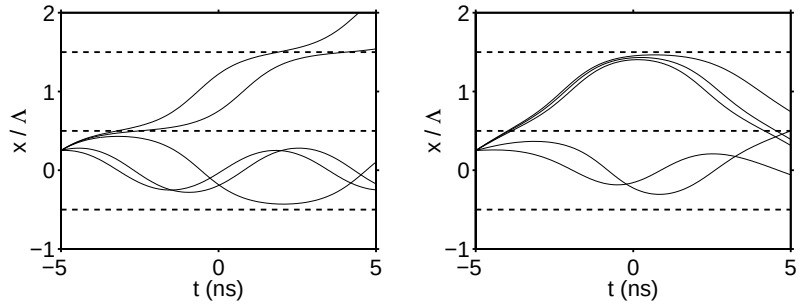

Figure 13: The differences in atomic motion in a pulsed standing wave with two types of temporal pulse profiles. (a) laser pulse with a fast turn on/off, (b) laser pulse with a Gaussian temporal profile. The curves represent trajectories of atoms at different initial velocities. The e^{-2} width of the Gaussian laser pulse and the lenght of the square-type laser pulse are both 10 ns. The pulse areas are equal in both cases.

the period of the standing-wave pattern. This is true also for the other reflection optima at which the particles will experience several oscillations in the potential well during the interaction time. To increase the reflection coefficient of the PSWM, the effective potential should be modified in such a way that the quadratic part around the antinodes (nodes) covers a wider region of each period of the standing-wave pattern. In the case of simple atoms, this can be done, for example, with the aid of a bichromatic standing wave [123], or by applying a magneto-optic potential [124], which in some cases can produce an almost perfectly quadratic potential over the whole period.

As far as elastic reflection is concerned, the first reflection optimum provides the maximum efficiency. In this case, the temporal profile of the laser pulse will not have a significant effect on the reflection characteristics of the PSWM [Paper V]. However, at higher intensities the pulse profile can have a considerable effect on the dynamics of the particles. In particular, the motion of fast particles ($v_\mathrm{i} \gtrsim \Lambda/2T$), which move in the anharmonic part of the potential, depends strongly on the temporal shape of the laser pulse (see Fig. 13). When using square-form laser pulses, particles can be captured only in the same period of the standing-wave pattern in which they are located at the turn-on time of the laser field. Furthermore, the capture efficiency approaches zero close to the nodes of the standing wave (attractive mode). In contrast, when using laser pulses with a smooth temporal profile, particles that start close to the nodes can still be captured by the neighbouring period of the standing-wave pattern. The reflection efficiency of the PSWM will then be optimized for particles that start in certain initial velocity groups. This will lead to a similar bifurcated final momentum distribution as a function of the initial velocity as is observed for atoms crossing a CW standing wave with a Gaussian spatial profile [125].

4.2.1 Reflection of neutral molecules

In Paper IV, we study the reflection of neutral molecules by pulsed standing waves with intensities of several tens of GW/cm^2. Such intensities can be generated relatively easily with many types of commercial pulsed laser systems. Here we choose the laser parameters according to typical values for pulsed Nd:YAG lasers. This is a convenient choice in the sense that single mode, high-power Nd:YAG lasers are readily available. Moreover, deflection and focusing of molecular beams have already been demonstrated using such lasers [104, 105], which provides an experimental proof on their suitability for the manipulation of neutral molecules.

In this thesis, we limit the discussion to linear molecules and linear polarization. Furthermore, we assume that the field intensity is high enough to cause alignment of the molecules along the polarization direction. In this case, the adiabatic rotational energy eigenvalues of the molecules take the simple form [102, 126]

$$U_{J,M} \approx -\frac{1}{4}\alpha_{\|}E_0^2(\vec{R},t) + E_0(\vec{R},t)\sqrt{B_e\Delta\alpha} \times (2J + |M| + 1), \qquad (31)$$

where J and M are, respectively, the total angular momentum of the molecule and its projection on the space-fixed z-axis defined by the polarization direction. If the electric field changes smoothly on the time scale of the rotational motion, the above eigenvalues can be used as the effective interaction potential for the molecules [103]. Since the rotational motion evolves on the time scale of $\hbar/B_{\mathrm{e}}$ [127], where B_{e} is the rotational constant, the condition of adiabaticity is typically fulfilled for laser pulses with a duration in the nanosecond regime.

As can be seen from Eq. (31), the first term in the effective potential is proportional to the intensity of the laser field, and the second term to the field amplitude. Due to this linear term, the effective potential will not be purely sinusoidal. However, a region with a nearly quadratic form can still be obtained at least at every second antinode of the standing wave. This means that the PSWM can be used as an elastic reflector for neutral molecules, but in a general case, its efficiency will be halved in comparison with the results of the previous subsection. However, at high intensities, i.e. for $\alpha_{\|}E_0(t)/(4\sqrt{B_e\Delta\alpha}) \gg 1$, and at low rotational temperatures, the second term in Eq. (31) can be neglected. In this case, the effective potential assumes a purely sinusoidal form and allows the regions around each antinode position of the standing wave to be utilized as an elastic reflector. This is the case, for example, for Rb dimers, for which the first reflection optimum occurs at intensities on the order of 30 GW/cm^2 when using laser pulses with a duration of 10 ns ($\alpha_{\|}E_0/(4\sqrt{B_e\Delta\alpha}) \approx 30$ at 30 GW/cm^2) [Paper IV].

The functioning of the PSWM as a molecule mirror is illustrated in Fig. 14 for the first reflection optimum. The distributions are calculated for laser pulses with a Gaussian temporal profile. The e^{-2} width of the laser pulse is 10 ns. Since the pulse duration

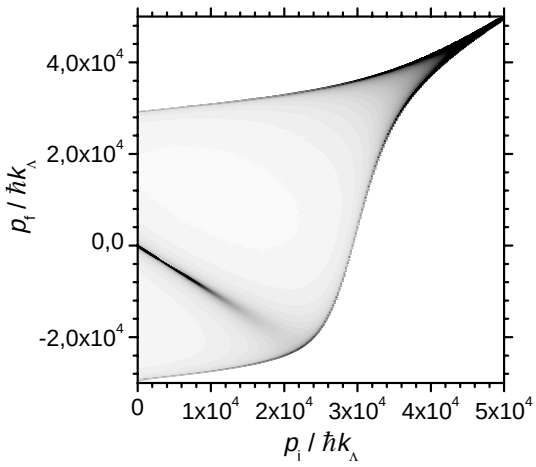

Figure 14: Gray-scale plot of the final momentum distribution of Rb_2 molecules as a function of the initial momentum in the case of a laser pulse with a Gaussian temporal profile. The e^{-2} width of the profile is 10 ns. The distribution corresponds to the first reflection optimum, i.e., to an oscillation period of $T_{\rm osc} \approx 2T$. Notice the dark line at -45 degrees indicating a strong elastic reflection of molecules with $p_i \lesssim 12000\,\hbar k_\Lambda$.

is much longer than the time scale for the rotational motion ($\hbar/B_{\rm e} \approx 200$ ps [128]), the adiabaticity is guaranteed at all times. As can be seen from Fig. 14, a significant fraction (ca. 20 %) of the incoming molecules in the range $v_i T \lesssim \Lambda/2$ (in this case $mv_{\rm i} \lesssim 12000\,\hbar k_\Lambda$) are reflected nearly elastically. The velocity limit can be increased by increasing the laser intensity and the period of the standing wave pattern. However, to reach the thermal velocities, very high intensities are required. For example, for $v_{\rm i} \approx 500$ m/s the required laser intensity is approximately 1 TW/cm^2. Such intensities can be reached by focusing a pulsed laser beam to a small spot. This will, however, lead to a reduction of the interaction volume. In addition, at high intensities the reflection efficiency will start to decrease due to multiphoton ionization.

The width of the momentum distribution of the elastically reflected molecules, δp, depends on how well the relation (30) is satisfied. In a realistic case, the laser intensity varies from pulse to pulse or may have a nonuniform spatial distribution. Consequently, the oscillation period will fluctuate around the optimum value, and the molecules will spread into a band around the final momentum state $p_f = -p_i$. For example, assuming $\pm$2% fluctuations in the intensity, the average width of the distribution of the elastically reflected molecules in Fig. 14 would be $\delta p \approx 200\,\hbar k_\Lambda$. Compared with the ability of the PSWM to reflect molecules with initial momenta as large as $p_i \lesssim 12000\hbar k_\Lambda$, this spread is, however, insignificant.

The results of our numerical calculations indicate that the PSWM can be used to efficiently control the center-of-mass motion of slow molecules ($v_i \lesssim 25$ m/s) at low

rotational temperatures. Such molecules have been produced recently with photoassociation in magneto-optical traps (e.g., for Rb_2 [129, 130]), with buffer-gas cooling of paramagnetic molecules [131, 132], and by using time-varying electric fields to decelerate molecular beams [133]. Evidently, the use of the PSWM to control the motion of these slow molecules will be of great interest in developing new types of optical applications with gas-phase molecules.

4.2.2 Reflection of thermal atoms

In Paper V, we study the use of the PSWM for reflection of two-level atoms in the limit of large detuning. We assume that external relaxation processes, such as spontaneous emission and phase fluctuations of the laser field, can be neglected. This is a reasonable assumption, since we are dealing with large detunings and short pulse durations. Futhermore, in practical experiments, single mode lasers can be used to reduce the effects of the phase fluctuations even on exact resonance. The effective potential seen by the atoms can be determined by using the dressed-state description for the two-level atoms (see, e.g., [134]). In this approach, the atom and the laser field are considered to form a combined system and the resulting eigenstates of the total Hamiltonian, the dressed states, are used to determine the effects of the laser field on the atomic motion. Assuming that nonadiabatic transitions between the dressed levels can be neglected, the eigenenergies of the dressed states can be used as the effective potential. They are [135]

$$U(x,t) = \frac{1}{2}\hbar\left[\Delta \pm \sqrt{\Delta^2 + \Omega(x,t)^2}\right], \tag{32}$$

where the signs refer to different dressed states. The Rabi frequency is defined as $\Omega(x,t) = \mu E_0(\vec{R},t)/\hbar$, where μ is the dipole matrix element for the transition. This model for the effective potential is valid, if $\Delta \gtrsim \Omega$ and if the laser field changes smoothly in time, e.g., $1/\delta t \ll |\Delta|$, where δt is the turn-on time of the laser pulse [135, 136].

At large detunings, the effective potential in Eq. (32) reduces to a sinusoidal form and, therefore, it can be applied as an elastic reflector for atoms with initial velocities up to $v_{\mathrm{i}}^{\max} \lesssim \Lambda/2T$. At typical parameter values for pulsed dye lasers, $T = 10$ ns and $\Lambda = 800$ nm, the velocity limit will be $v_{\mathrm{i}}^{\max} \approx 40$ m/s. The corresponding intensity for the first reflection optimum is approximately 100 MW/cm^2 when using atomic parameters corresponding to the sodium D_2 transition. Such intensities can be reached relatively easily with many types of pulsed dye laser systems and should not cause significant difficulties in practical applications. For some atomic species multiphoton ionization can, however, reduce the reflection efficiency already at this intensity.

As compared with the conventional atom mirror geometries, the PSWM can be used to reflect atoms with an order of magnitude higher initial velocities. This allows the

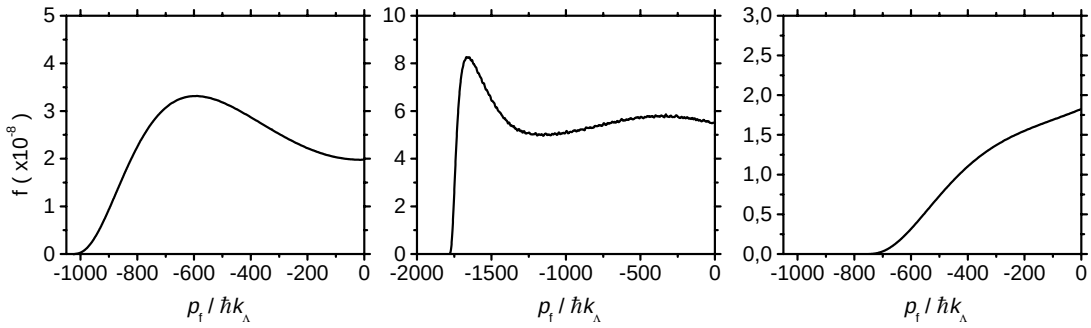

Figure 15: The final momentum distribution of a thermal beam of sodium atoms after interaction with a pulsed standing wave. The distributions are calculated using laser pulses with a fast turn on/off and a duration of 10 ns. For (a) $\Omega_0 = 3.4 \times 10^{12}\,\mathrm{s}^{-1}$ ($T_{osc} \approx 19$ ns), (b) $\Omega_0 = 1 \times 10^{13}\,\mathrm{s}^{-1}$ ($T_{osc} \approx 11$ ns), and (c) $\Omega_0 = 2 \times 10^{12}\,\mathrm{s}^{-1}$ ($T_{osc} \approx 25$ ns). The detuning is $\Delta = 5\Omega_0$ in all cases. The period of the standing-wave pattern is 294.5 nm. The vertical axis gives the fraction of atoms that end up in a final momentum state $m\hbar k_\Lambda$, where m is an integer.

PSWM to be applied to control the motion of thermal atomic beams, for which the traditional atom mirrors work only at grazing incidence. Furthermore, the large interaction volume of the PSWM allows an experimentally useful number of atoms to be reflected from a thermal beam even at normal incidence. For example, more than 10^4 atoms/cm can be reflected from a thermal beam of sodium atoms already at an intensity of 10 MW/cm^2 ($v_\mathrm{i}^\mathrm{max} = 15$ m/s, $\Lambda = 294.5$ nm) [Paper V]). The number of reflected atoms will be increased by an order of magnitude at an intensity of 100 MW/cm^2.

Since the atomic dynamics in a pulsed standing wave strongly depends on the ratio of the oscillation period to the interaction time, the shape of the final momentum distribution depends on the value of the Rabi frequency. At non-optimal values of the oscillation period the atoms will spread to a wide range of momentum states and, consequently, the reflection efficiency of the PSWM is significantly reduced. However, it turns out that the number of atoms in negative momentum states can still be high. This offers the possibilities to use the PSWM as an inelastic reflector, and to modify the momentum distribution of the reflected atoms. For example, in Fig. 15 we show final momentum distributions around the first reflection optimum. We illustrate generation of slow atoms, or a nearly flat momentum distribution. These distributions correspond to laser pulses with a square temporal profile.

In addition to the pulse duration, the shape of the laser pulse can have a significant effect on the shape of the final momentum distributions. This is illustrated in Fig. 16

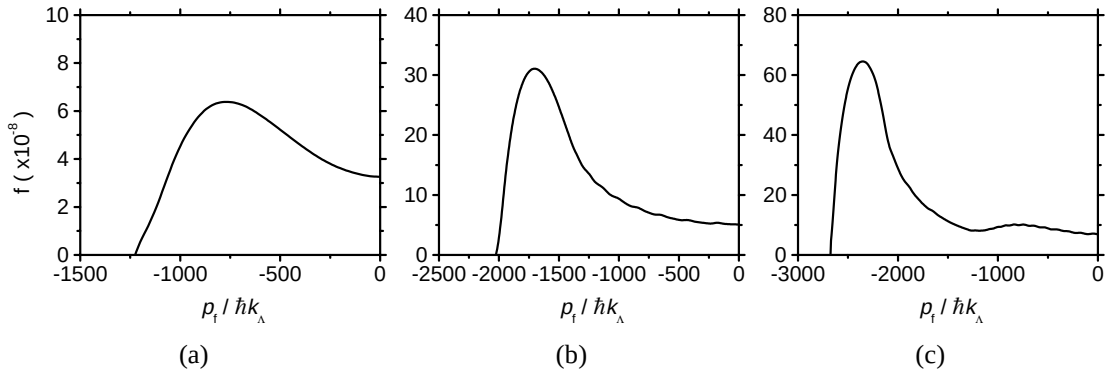

Figure 16: The final momentum distribution of a thermal beam of sodium atoms after interaction with a pulsed standing wave. The distributions are calculated using laser pulses with a Gaussian temporal profile. The e^{-2} width of the Gaussian profile is 10 ns. For (a) $\Omega_0 = 7.7 \times 10^{12}\,\mathrm{s}^{-1}$, (b) $\Omega_0 = 2.4 \times 10^{13}\,\mathrm{s}^{-1}$, and (c) $\Omega_0 = 4.6 \times 10^{13}\,\mathrm{s}^{-1}$. The period of the standing-wave pattern is 294.5 nm. The vertical axis gives the fraction of atoms that end up in a final momentum state $m\hbar k_\Lambda$, where m is an integer.

for laser pulses with a Gaussian temporal profile. In Fig. 16(a), the intensity is chosen such that the fraction of the elastically reflected atoms is optimized. In this case, the temporal profile of the pulse does not have a significant effect on the reflection dynamics, and the final momentum distribution turns out to be similar to that in Fig. 15(a). The main difference is that the first reflection optimum occurs at a slightly higher peak intensity than was found for the case of the square-profile laser pulse. This is due to the fact that the maximum momentum that can be transferred to the atoms increases more slowly as a function of the field intensity for a smooth pulse than for a pulse that turns on abruptly [137].

At higher intensities ($T_{\mathrm{osc}} \lesssim T$), the pulse profile will have a more significant influence on the shape of the final momentum distribution. In Fig. 16(b), the field intensity was increased to give $T_{\mathrm{osc}} \approx T$. In this case, the slow atoms that move in the most harmonic part of the effective potential are transmitted and thus the low negative momentum states are only slightly populated. However, the standing wave can still reflect certain anharmonically moving atoms that have a suitable initial velocity. These atoms pile up in the high-negative momentum states of the final distribution, as shown in Fig. 16(b). Figure 16(c) corresponds to the second reflection optimum ($n = 2$) for the harmonically moving atoms. In this case, the shape of the final momentum distribution at low momentum states is again similar to that of Fig. 15(a), and the anharmonically reflected atoms have moved to higher negative momentum states. At still higher intensities, the distribution aquires more maxima corresponding to the different initial velocity groups that can be reflected. Since the maxima are located at high momentum states, the shape of the final momentum distribution seems to be more difficult to

control when using smooth laser pulses than it was in the case of square-profile pulses.

The control of the final momentum distribution can be improved by using a standing-wave pattern that moves with a velocity of $v_{\rm sw}$. In this case, the atoms are reflected with respect to the momentum $mv_{\rm sw}$ [Paper V]. Therefore, by varying the velocity of the moving standing-wave pattern, the final momentum of the reflected atoms can be chosen appropriately. In particular, with a suitable choice of $v_{\rm sw}$, the peak in Fig. 16(b)-(c) can be moved to zero momentum. The scheme of the moving standing-wave pattern might, therefore, be interesting, for example, for the generation of slow atoms in cases where the normal laser cooling methods are inefficient. This could include multilevel atoms, or at somewhat higher intensities even molecules. Furthermore, by applying a few moving standing-wave pulses in succession, it might also be possible to transfer fast atoms or molecules to low momentum states even at moderate laser intensities.

5 Conclusions

In this thesis, the use of pulsed laser fields to control the center-of-mass motion of neutral atoms and molecules is studied both numerically and experimentally. In particular, we consider the use of a pulsed standing wave for the deflection of atomic beams, and develop novel types of mirrors for applications in atom and molecule optics. The research work shows that pulsed laser fields can be applied to form efficient mirrors for neutral particles regardless of the details of their internal energy-level structure. Moreover, it is shown that pulsed standing waves can also be utilized to efficiently deflect atomic beams.

In the first part of the thesis, we study the effects of phase fluctuations of the laser field on the momentum distribution of atoms after interaction with a standing wave. Our numerical simulations show that the coherence properties of the laser field play a major role in diffraction of atoms, especially when using pulsed lasers. It turns out that the effects caused by the limited coherence time of the optical field are clearly observable as a transfer of atoms in momentum space to the region around zero momentum rather than to high momentum states. For the typical bandwidth values of multimode dye lasers the deflection appears to be mainly diffusive. The occupation of the momentum states on the wings of the double-peaked Bessel function distribution, i.e., the number of atoms with large deflection angles, can be increased by reducing the spectral width of the light field closer to the Fourier limit. However, even with narrow bandwidths the diffusive component will still be observable, which indicates the importance of phase fluctuations in the diffraction experiments.

The numerical analysis of the pulsed standing-wave diffraction was complemented by experimental measurements of the deflection profiles of a beam of thermal sodium atoms. The experimental distributions were measured for a value of the coherence time intermediate between the Rabi period and the interaction time. The observed distribution of final momenta was found to be in a reasonable agreement with the theoretical predictions. A comparison of the results with an expected distribution calculated for a fully coherent interaction shows that the phase fluctuations of the light field drastically affect the achievable transverse momentum values. Based on our theoretical and experimental analysis of the diffraction profiles, we conclude that large deflection angles can be reached only when laser pulses with a Fourier-limited bandwidth are applied.

The second part of the thesis concentrates on the development of pulsed mirrors for neutral atoms and molecules. In particular, we consider the use of an evanescent wave, formed in total internal reflection of light on a vacuum-dielectric interface, and of a standing wave as possible mirror configurations. Our numerical simulations of the pulsed evanescent-wave mirror show that atoms with initial velocities up to several tens of meters per second can be reflected already at the moderate field intensities of a few tens of MW/cm^2. This allows pulsed evanescent waves to be applied in a compact

setup to control the motion of thermal atomic beams, for which the traditional atom mirrors are suited only at grazing incidence. However, since the effective interaction volume of the atomic beam and the laser field is limited by the short decay length of the evanescent wave, only a relatively small number of atoms can be reflected with a single laser pulse. Furthermore, the reflection is always inelastic, since the force exerted on the atoms varies as a function of the initial position of the particles. To solve the above problem we consider the use of a standing wave as a pulsed mirror for atoms. Our numerical simulations show that with a proper choice of the pulse duration and field intensity, each period of the standing-wave pattern functions as an elastic mirror for particles with an initial kinetic energy below the depth of the standing-wave potential. Hence, the standing-wave pattern acts as a long row of independent atom mirrors, which provides a novel route to controlling large volumes of fast atoms even with a single laser pulse.

As a second application for the pulsed standing-wave mirror we consider the reflection of slow molecules, for which no efficient mirror configuration previously has been available. It is shown that pulsed standing waves of nonresonant frequencies can be used to efficiently manipulate large volumes of rotationally cold molecules. With a suitable choice of the parameter values, the molecules can be reflected nearly elastically, or with a tailored momentum distribution. This opens up a possibility to use the pulsed standing-wave mirror to control the motion of particles in various applications of atomic and molecular physics. Such a mirror could be applied, for example, to steer and image molecular beams, separate molecular species, and to form pulsed molecular beams.

In conclusion, the research work in this thesis shows that the use of pulsed laser fields offers certain advantages in devising components for atom optics. In particular, the possibility to control the motion of neutral gas-phase molecules with the pulsed standing-wave mirror shows up as a promising tool for the emerging field of molecule optics. Apparently, following the recent advances in cooling and trapping of neutral molecules, the interest in such a component will grow in the near future.

References

[1] C. Davidson and L. H. Germer, "Diffraction of Electrons by a Crystal of Nickel", *Phys. Rev.* **30**, 705–740 (1927).

[2] O. Stern, "Beugung von Molekularstrahlen an Gitter einer Krystallspaltfläche", *Naturwiss.* **17**, 391 (1929).

[3] I. Esterman and O. Stern, "Beugung von Molekularstrahlen", *Z. Physik* **61**, 95–125 (1930).

[4] E. Brüche and H. J. Johannson, "Elektronenoptik und Elektronenmikroskop", *Naturwiss.* **20**, 353–358 (1932).

[5] H. Friedburg, "Optische Abbildung mit Neutralen Atomen", *Z. Physik.* **130**, 492–512 (1951).

[6] H. Friedburg and W. Paul, "Optische Abbildung mit Neutralen Atomen", *Naturwiss.* **38**, 159–160 (1951).

[7] J. A. Leavitt and F. A. Bills, "Single-Slit Diffraction Pattern of a Thermal Atomic Potassium Beam", *Am. J. Phys.* **37**, 905–912 (1969).

[8] A. Ashkin, "Atomic-Beam Deflection by Resonance-Radiation Pressure", *Phys. Rev. Lett.* **25**, 1321–1324 (1970).

[9] R. Schieder, H. Walther, and L. Wöste, "Atomic Beam Deflection by the Light of a Tunable Dye Laser", *Opt. Commun.* **5**, 337–340 (1972).

[10] J.-L. Picque and J.-L. Vialle, "Atomic-Beam Deflection and Broadening by Recoils due to Photon Absorption or Emission", *Opt. Commun.* **5**, 402–406 (1972).

[11] R. J. Cook and A. F. Bernhardt, "Deflection of Atoms by a Resonant Standing Electromagnetic Wave", *Phys. Rev. A* **18**, 2533–2537 (1978).

[12] E. Arimondo, H. Lew, and T. Oka, "Deflection of a Na Beam by Resonant Standing-Wave Radiation", *Phys. Rev. Lett.* **43**, 753–756 (1979).

[13] T. W. Hänsch, "Cooling of Gases by Laser Radiation", *Opt. Commun.* **13**, 68–69 (1975).

[14] V. S. Letokhov, V. G. Minogin, and B. D. Pavlik, "Cooling and Trapping of Atoms and Molecules by a Resonant Laser Field", *Opt. Commun.* **19**, 72–75 (1976).

[15] E. V. Baklanov and B. Ya. Dubetskii, "Fokker-Plank Equation for Gas Atoms Resonantly Interacting with a Light Wave", *Opt. Spectrosc.* **41**, 1–4 (1976).

[16] S. Stenholm and J. Javanainen, "Velocity Redistribution by Standing Waves", *Appl. Phys.* **16**, 159–166 (1978).

[17] V. I. Balykin, V. S. Letokhov, and V. I. Mushin, "Observation of the Cooling of Free Sodium Atoms in a Resonance Laser Field with a Scanning Frequency", *JETP Lett.* **29**, 560–564 (1979).

[18] A. P. Gaponov and M. A. Miller, "Potential Wells for Charged Particles in a High-Frequency Electromagnetic Field", *Sov. Phys. JETP* **7**, 168–169 (1958).

[19] V. S. Letokhov, "Narrowing of the Doppler Width in a Standing Light Wave", *JETP Lett.* **7**, 272–275 (1968).

[20] A. P. Kazantsev, "Acceleration of Atoms by a Resonance Field", *Sov. Phys. JETP* **36**, 861–864 (1973).

[21] A. Ashkin, "Trapping of Atoms by Resonance Radiation Pressure", *Phys. Rev. Lett.* **40**, 729–732 (1978).

[22] A. F. Bernhardt, D. E. Duerre, J. R. Simpson, and L. L. Wood, "Separation of Isotopes by Laser Deflection of Atomic Beam. I. Barium", *Appl. Phys. Lett.* **25**, 617–620 (1974).

[23] A. F. Bernhardt, D. E. Duerre, J. R. Simpson, and L. L. Wood, "Multifrequency Radiation Pressure Laser, Isotope Separation", *Opt. Commun.* **16**, 169–171 (1976).

[24] J. Javanainen, "Separation of Atomic Beams by Light Pressure", *Appl. Phys.* **21**, 263–269 (1980).

[25] A. Ashkin, "Acceleration and Trapping of Particles by Radiation Pressure", *Phys. Rev. Lett.* **24**, 156–158 (1970).

[26] A. Ashkin and J. M. Dziedzic, "Optical Levitation by Radiation Pressure", *Appl. Phys. Lett.* **19**, 283–285 (1971).

[27] P. Jacquinot, S. Liberman, J.-L. Picqué, and J. Pinard, "High Resolution Spectroscopic Application of Atomic Beam Deflection by Resonant Light", *Opt. Commun.* **8**, 163–165 (1973).

[28] S. Stenholm, "Recoil Effects in Quantum Electronics: The Nonlinear Molecular Response", *J. Phys. B* **7**, 1235–1254 (1974).

[29] J. L. Hall, C. J. Bordé, and K. Uehara, "Direct Optical Resolution of the Recoil Effect Using Saturated Absorption Spectroscopy", *Phys. Rev. Lett.* **37**, 1339–1342 (1976).

[30] E. L. Raab, M. Prentiss, A. Cable, S. Chu, and D. E. Pritchard, "Trapping of Neutral Sodium Atoms with Radiation Pressure", *Phys. Rev. Lett.* **59**, 2631–2634 (1987).

[31] M. H. Anderson, J. R. Ensher, M. R. Matthews, C. E. Wieman, and E. A. Cornell, "Observation of Bose-Einstein Condensation in a Dilute Atomic Vapor", *Science* **269**, 198–201 (1995).

[32] C. C. Bradley, C. A. Sackett, J. J. Tollett, and R. G. Hulet, "Evidence of Bose-Einstein Condensation in an Atomic Gas with Attractive Interactions", *Phys. Rev. Lett.* **75**, 1687–1690 (1995); *Phys. Rev. Lett.* **79**, 1170 (1997).

[33] K. B. Davis, M.-O. Mewes, M. R. Andrews, N. J. van Druten, D. S. Durfee, D. M. Kurn, and W. Ketterle, "Bose-Einstein Condensation in a Gas of Sodium Atoms", *Phys. Rev. Lett.* **75**, 3969–3973 (1995).

[34] O. Carnal and J. Mlynek, "Young's Double Slit Experiment with Atoms: A Simple Atom Interferometer", *Phys. Rev. Lett.* **66**, 2689–2692 (1991).

[35] D. W. Keith, C. R. Ekstrom, W. A. Turchette, and D. E. Pritchard, "An Interferometer for Atoms", *Phys. Rev. Lett.* **66**, 2693–2696 (1991).

[36] M. Kasevich and S. Chu, "Atomic Interferometry Using Stimulated Raman Transitions", *Phys. Rev. Lett.* **67**, 181–184 (1991).

[37] F. Riehle, Th. Kisters, A. Witte, and J. Helmcke, "Optical Ramsey Spectroscopy in a Rotating Frame: Sagnac Effect in a Matter-Wave Interferometer", *Phys. Rev. Lett.* **67**, 177–180 (1991).

[38] C. Salomon, J. Dalibard, A. Aspect, H. Metcalf, and C. Cohen-Tannoudji, "Channeling Atoms in a Laser Standing Wave", *Phys. Rev. Lett.* **59**, 1659–1662 (1987).

[39] G. Timp, R. E. Behringer, D. M. Tennant, and J. E. Cunningham, "Using Light as a Lens for Submicron and Neutral-Atom Lithography", *Phys. Rev. Lett.* **69**, 1636–1639 (1992).

[40] J. J. McClelland, R. E. Scholten, E. C. Palm, and R. J. Celotta, "Laser-Focused Atomic Deposition", *Science* **262**, 877–880 (1993).

[41] R. B. Doak, R. E. Grisenti, S. Rehbein, G. Schmahl, J. P. Toennies, and Ch. Wöll, "Towards Realization of an Atomic de Broglie Microscopy: Helium Atom Focusing Using Fresnel Zone Plates", *Phys. Rev. Lett.* **83**, 4229–4232 (1999).

[42] M.-O. Mewes, M. R. Andrews, D. M. Kurn, D. S. Durfee, C. G. Townsend, and W. Ketterle, "Output Coupler for Bose-Einstein Condensed Atoms", *Phys. Rev. Lett.* **78**, 582–585 (1997).

[43] M. R. Andrews, C. G. Townsend, H.-J. Miesner, D. S. Durfee, D. M. Kurn, and W. Ketterle, "Observation of Interference Between Two Bose Condensates", *Science* **275**, 637–641 (1997).

[44] S. Inouye, T. Pfau, S. Gupta, A. P. Chikkatur, A. Gorlitz, D. E. Pritchard, and W. Ketterle, "Phase-Coherent Amplification of Atomic Matter Waves", *Nature* **402**, 641–644 (1999).

[45] L. Deng, E. W. Hagley, J. Wen, M. Trippenbach, Y. Band, P. S. Julienne, J. E. Simsarian, K. Helmerson, S. L. Rolston, and W. D. Phillips, "Four-Wave Mixing with Matter Waves", *Nature* **398**, 218–220 (1999).

[46] S. Stenholm, "The Semiclassical Theory of Laser Cooling", *Rev. Mod. Phys.* **58**, 699–739 (1986).

[47] R. W. Boyd, *Nonlinear Optics* (Academic Press, New York, 1992).

[48] R. J. Cook, "Atomic Motion in Resonant Radiation: An Application of Ehrenfest's Theorem", *Phys. Rev. A* **20**, 224–228 (1979).

[49] C. Tanguy, S. Reynaud, and C. Cohen-Tannoudji, "Deflection of an Atomic Beam by a Laser Wave: Transition Between Diffractive and Diffuusive Regimes", *J. Phys. B: At. Mol. Phys.* **17**, 4623–4641 (1984).

[50] S. Stenholm, "Distribution of Photons and Atomic Momentum in Resonance Fluorescence", *Phys. Rev. A* **27**, 2513–2522 (1983).

[51] E. Wigner, "On the Quantum Correction For Thermodynamic Equilibrium", *Phys. Rev.* **40**, 749–759 (1932).

[52] O. Carnal, M. Siegel, T. Sleator, H. Takuma, and J. Mlynek, "Imaging and Focusing of Atoms by a Fresel Zone Plate", *Phys. Rev. Lett.* **67**, 2131–3234 (1991).

[53] D. W. Keith, M. L. Schattenburg, H. I. Smith, and D. E. Pritchard, "Diffraction of Atoms by Transmission Grating", *Phys. Rev. Lett.* **61**, 1580–1583 (1988).

[54] M. Morinaga, M. Yasuda, T. Kishimoto, and F. Shimizu, "Holographic Manipulation of a Cold Atomic Beam", *Phys. Rev. Lett.* **77**, 802–805 (1996).

[55] S. Altschuler and L. M. Frantz, "Reflection of Atoms from Standing Light Waves", *Phys. Rev. Lett.* **17**, 231–232 (1966).

[56] A. P. Kazantsev and G. I. Surdutovich, "The Kapitza-Dirac Effect for Atoms in a Strong Resonant Field", *JETP Lett.* **21**, 158–159 (1975).

[57] G. A. Delone, V. A. Grinchuk, A. P. Kazantsev, and G. I. Surdutovich, "Scattering of Atoms and Molecules by an Electromagnetic Field", *Opt. Commun.* **25**, 399–401 (1978).

[58] G. A. Delone, V. A. Grinchuk, S. D. Kuzmichev, M. L. Nagaeva, A. P. Kazantsev, and G. I. Surdutovich, "The Kapitsa-Dirac Resonance Effect", *Opt. Commun.* **33**, 149–152 (1980).

[59] V. A. Grinchuk, A. P. Kazantsev, E. F. Kuzin, M. L. Nagaeva, G. A. Ryabenko, G. I. Surdutovich, and V. P. Yakovlev, "Scattering of Atoms by a Short and Standing-Light-Wave Pulse", *JETP Lett.* **34**, 375–378 (1981).

[60] V. G. Minogin, "Atomic Scattering by a Resonant Standing Light Wave", *Opt. Commun.* **37**, 442–446 (1982).

[61] C. Tanguy, S. Reynaud, M. Matsuoka, and C. Cohen-Tannoudji, "Deflection Profiles of a Monoenergetic Atomic Beam Crossing a Standing Light Wave", *Opt. Commun.* **44**, 249–253 (1983).

[62] P. E. Moskowitz, P. L. Gould, and D. E. Pritchard, "Deflection of Atoms by Standing-Wave Radiation", *J. Opt. Soc. Am. B* **2**, 1784–1789 (1985).

[63] P. Gould, G. Ruff, and D. Pritchard, "Diffraction of Atoms by Light: The Near-Resonant Kapitza-Dirac Effect", *Phys. Rev. Lett.* **56**, 827–830 (1986).

[64] P. L. Gould, P. J. Martin, G. A. Ruff, R. E. Stoner, J.-L. Picqué, and D. E. Pritchard, "Momentum transfer to Atoms by a Standing Light Wave: Transition from Diffraction to Diffusion", *Phys. Rev. A* **43**, 585–588 (1991).

[65] T. Pfau, S. Spälter, Ch. Kurtsiefer, C. R. Ekstrom, and J. Mlynek, "Loss of Spatial Coherence by a Single Spontaneous Emission", *Phys. Rev. Lett.* **73**, 1223–1226 (1994).

[66] V. A. Grinchuk, E. F. Kuzin, M. L. Nagaeva, G. A. Ryabenko, A. P. Kazantsev, G. I. Surdutovich, and V. P. Yakovlev, "Scattering of Atoms by Coherent Interaction with Light", *J. Opt. Soc. Am. B* **2**, 1805–1813 (1985).

[67] J. Dalibard and Y. Castin, "Wave-Function Approach to Dissipative Processes in Quantum Optics", *Phys. Rev. Lett.* **68**, 580–583 (1992).

[68] A. P. Kazantsev, G. I. Surdutovich, and V. P. Yakovlev, "On the Quantum Theory of Resonance Scattering of Atoms by Light", *JETP Lett.* **31**, 511–513 (1980).

[69] A. F. Bernhardt and B. W. Shore, "Coherent Atomic Deflection by Resonant Standing Wave", *Phys. Rev. A* **23**, 1290–1301 (1981).

[70] E. Arimondo, A. Bambini, and S. Stenholm, "Quasiclassical Theory of Laser-Induced Atomic-Beam Dispersion", *Phys. Rev. A* **24**, 898–909 (1981).

[71] T. Sleator, T. Pfau, V. Balykin, O. Carnal, and J. Mlynek, "Experimental Demonstration of the Optical Stern-Gerlach Effect", *Phys. Rev. Lett.* **68**, 1996–1999 (1992).

[72] P. Martin, B. Oldaker, A. Miklich, and D. Pritchard, "Bragg Scattering of Atoms from a Standing Wave", *Phys. Rev. Lett.* **60**, 515–518 (1988).

[73] B. W. Hendriks and G. Nienhaus, "Diffraction of an Atomic Beam by a Phase-Fluctuating Standing Light Wave", *Phys. Rev. A* **36**, 5615–5625 (1987).

[74] J. H. Eberly, "Atomic Relaxation in the Presence of Intense Coherent Radiation Fields", *Phys. Rev. Lett.* **37**, 1387–1390 (1976).

[75] G. S. Agarwal, "Exact Solution for the Influence of Laser Temporal Fluctuations on Resonance Fluorescence", *Phys. Rev. Lett.* **37**, 1383–1386 (1976).

[76] P. Zoller, "Fokker-Plank Equation Treatment of Atomic Relaxation and Resonance Fluerescence in Phase-Modulated Laser Light", *J. Phys. B: At. Mol. Phys.* **10**, L321–L324 (1977).

[77] G. S. Agarwal, "Quantum Statistical Theory of Optical-Resonance Phenomena in Fluctuating Laser Fields", *Phys. Rev. A* **18**, 1490–1506 (1978).

[78] J. H. Eberly, K. Wódkiewicz, and B. W. Shore, "Noise in Strong Laser-Atom Interactions: Phase Telegraph Noise", *Phys. Rev. A* **30**, 2381–2389 (1984).

[79] K. Wódkiewicz, B. W. Shore, and J. H. Eberly, "Noise in Strong Laser-Atom Interactions: Frequency Fluctuations and Nonexponential Correlations", *Phys. Rev. A* **30**, 2390–2398 (1984).

[80] H. F. Arnoldus and G. Nienhuis, "Atomic Response to the Lorentz Wave", *J. Phys. B: At. Mol. Phys.* **19**, 873–881 (1986).

[81] R. J. Cook, "Atomic Motion in Resonant Fluctuating Laser Radiation", *Phys. Rev. A* **21**, 268–273 (1980).

[82] W. L. Wiese, M. W. Smith, and B. M. Glennon, *Atomic Transition Probabilities: a Critical Data Compilation*, Vol. 22 of *National standard reference data series* (U.S. Goverment Printing Office, Washington D.C., 1969).

[83] F. Knauer and O. Stern, "Über die Reflection von Molekularstrahlen", *Z. Physik* **53**, 779–791 (1929).

[84] R. Cook and R.K. Hill, "An Electromagnetic Mirror for Neutral Atoms", *Opt. Commun.* **43**, 258–260 (1982).

[85] V. I. Balykin, V. S. Letokhov, Yu. B. Ovchinnikov, and I. Sidorov, "Reflection of an Atomic Beam from a Gradient of an Optical Field", *JETP Lett.* **45**, 353–356 (1987).

[86] M. A. Kasevich, D. S. Weiss, and S. Chu, "Normal-Incidence Reflection of Slow Atoms from an Optical Evanecent Wave", *Opt. Lett.* **15**, 607 (1990).

[87] Yu. B. Ovchinnikov, I. Manek, A. I. Sidorov, G. Wasik, and R. Grimm, "Gravito-Optical Atom Trap Based on a Conical Hollow Beam", *Europhys. Lett.* **43**, 510–515 (1998).

[88] C. Henkel, C. I. Westbrook, and A. Aspect, "Quantum Reflection: Atomic Matter-Wave Optics in an Attractive Exponential Potential", *J. Opt. Soc. Am. B* **13**, 233–243 (1996).

[89] V. S. Letokhov and V. G. Minogin, "Quantum Motions of Ultracooled Atoms in Resonant Laser Field", *Phys. Lett.* **61A**, 370–372 (1977).

[90] V. S. Letokhov and V. G. Minogin, "Quantum Motion of Atoms in the Resonant Field of a Standing Light Wave", *Sov. Phys. JETP* **47**, 690–699 (1978).

[91] L. Santos and L. Roso, "Multilayer 'Dielectric' Mirror for Atoms", *Phys. Rev. A* **58**, 2407–2412 (1998).

[92] N. Friedman, R. Ozeri, and N. Davidson, "Quantum Reflection of Atoms from a Periodic Dipole Potential", *J. Opt. Soc. Am. B* **15**, 1749–1755 (1998).

[93] C. G. Aminoff, A. M. Steane, P. Bouyer, P. Desbiolles, J. Dalibard, and C. Cohen-Tannoudji, "Cesium Atoms Bouncing in a Stable Gravitational Cavity", *Phys. Rev. Lett.* **8**, 3083–3086 (1993).

[94] M. A. Ol'Shanii, Yu. B Ovchinnikov, and V. S. Letokhov, "Laser Guiding of Atoms in a Hollow Optical Fiber", *Opt. Commun.* **98**, 77–79 (1993).

[95] M. J. Renn, D. Montgomery, O. Vdovin, D. Z. Anderson, C. E. Wieman, and E. A. Cornell, "Laser-Guided Atoms in Hollow-Core Optical Fibers", *Phys. Rev. Lett.* **75**, 3253–3256 (1995).

[96] P. Szriftgiser, D. Guéry-Odelin, M. Arndt, and J. Dalibard, "Atomic Wave Diffraction and Interference Using Temporal Slits", *Phys. Rev. Lett.* **77**, 4–7 (1996).

[97] S. Feron, J. Reinhardt, S. Le Boiteux, O. Gorceix, J. Baudon, M. Ducloy, J. Robert, Ch. Miniatura, S. Nic Chormaic, H. Haberland, and V. Lorent, "Reflection of Metastable Neon Atoms by Surface Plasmon Wave", *Opt. Commun.* **83**, 83–88 (1993).

[98] T. Esslinger, M. Weidemüller, A. Hemmerich, and T. W. Hänsch, "Surface-Plasmon Mirror for Atoms", *Opt. Lett.* **18**, 450–452 (1993).

[99] R. Kaiser, Y. Levy, N. Vansteenkiste, A. Aspect, W. Seifert, D. Leipold, and J. Mlynek, "Resonant Enhancement of Evanescent Waves with a Thin Dielectric Waveguide", *Opt. Commun.* **104**, 234–240 (1994).

[100] W. Seifert, C. S. Adams, V. I. Balykin, C. Heine, Yu. B. Ovchinnikov, and J. Mlynek, "Reflection of Metastable Argon Atoms from an Evanescent Wave", *Phys. Rev. A* **49**, 3814–3823 (1994).

[101] V. S. Voĭtsekhovich, M. L. Danileĭko, A. M. Negriĭko, V. I. Romanenko, and L. P. Yatsenko, "Observation of Radiation Pressure Exerted on Molecules", *JETP Lett.* **59**, 411 (1994).

[102] B. Friedrich and D. Herschbach, "Alignment and Trapping of Molecules in Intense Laser Fields", *Phys. Rev. Lett.* **74**, 4623–4626 (1995).

[103] T. Seideman, "Shaping Molecular Beams with Intense Light", *J. Chem. Phys.* **107**, 10420–10429 (1997).

[104] H. Stapelfeldt, H. Sakai, E. Constant, and P. B. Corkum, "Deflection of Neutral Molecules using the Nonresonant Dipole Force", *Phys. Rev. Lett.* **79**, 2787–2790 (1997).

[105] H. Sakai, A. Tarasevitch, J. Danilov, H. Stapelfeldt, R. W. Yip, C. Ellert, E. Constant, and P. B. Corkum, "Optical Deflection of Molecules", *Phys. Rev. A* **57**, 2794–2801 (1998).

[106] V. I. Balykin, V. S. Letokhov, Yu. B. Ovchinnikov, and A. I. Sidorov, "Quantum-State Selective Mirror for Reflection of Atoms by Laser Light", *Phys. Rev. Lett.* **60**, 2137–2140 (1988).

[107] J. V. Hajnal and G. I. Opat, "Diffraction of Atoms by a Standing Evanescent Light Wave - A Reflection Grating for Atoms", *Opt. Commun.* **71**, 119–124 (1989).

[108] J. V. Hajnal, K. G. H. Baldwin, P. T. H. Fisk, H.-A. Bachor, and G. I. Opat, "Reflection and Diffraction of Sodium Atoms by Evanescent Laser Light Fields", *Opt. Commun.* **73**, 331–336 (1989).

[109] R. Deutschmann, W. Ertmer, and H. Wallis, "Reflection and Diffraction of Atomic de Broglie Waves by an Evanescent Laser Wave", *Phys. Rev. A* **47**, 2169–2185 (1993).

[110] S. Feron, J. Reinhardt, M. Ducloy, S. Nic Chormaic, C. Miniatura, J. Robert, J. Baudon, and V. Lorent, "Doppler-Tuned Multiphoton Resonances in an Atom Reflection by a Standing Evanescent Wave", *Phys. Rev. A* **49**, 4733–4741 (1994).

[111] L. Cognet, V. Savalli, G. Zs. K. Horvath, D. Holleville, R. Marani, N. Westbrook, C. I. Westbrook, and A. Aspect, "Atomic Interference in Grazing Incidence Diffraction from an Evanescent Wave Mirror", *Phys. Rev. Lett.* **81**, 5044–5047 (1998).

[112] S. Marksteiner, C. M. Savage, P. Zoller, and S. L. Rolston, "Coherent Atomic Waveguides from Hollow Optical Fibers: Quantized Atomic Motion", *Phys. Rev. A* **50**, 2680–2690 (1994).

[113] M. J. Renn, E. A. Donley, E. A. Cornell, C. E. Wieman, and D. Z. Anderson, "Evanescent-Wave Guiding of Atoms in Hollow Optical Fibers", *Phys. Rev. A* **53**, R648–R651 (1996).

[114] V. I. Balykin and V. S. Letokhov, "Atomic Cavity with Light-Induced Mirrors", *Appl. Phys. B* **48**, 517–523 (1989).

[115] H. Wallis, J. Dalibard, and C. Cohen-Tannoudji, "Trapping Atoms in a Gravitational Cavity", *Appl. Phys. B* **54**, 407–419 (1992).

[116] Yu. B. Ovchinnikov, D. V. Laryushin, V. I. Balykin, and V. S. Letokhov, "Cooling of Atoms by Reflection from a Surface Light Wave", *JETP Lett.* **62**, 113–118 (1995).

[117] Yu. B. Ovchinnikov, J. Söding, and R. Grimm, "Cooling Atoms in Dark Gravitational Laser Traps", *JETP Lett.* **61**, 21–26 (1995).

[118] J. Söding, R. Grimm, and Yu. B. Ovchinnikov, "Gravitational Laser Trap for Atoms with Evanescent Wave Cooling", *Opt. Commun.* **119**, 652–662 (1995).

[119] P. Desbiolles, M. Arndt, P. Szriftgiser, and J. Dalibard, "Elementary Sisyphus Process Close to a Dielectric Surface", *Phys. Rev. A* **54**, 4293–4298 (1996).

[120] Yu. B. Ovchinnikov, I. Manek, and R. Grimm, "Surface Trap for Cs Atoms Based on Evanescent Wave Cooling", *Phys. Rev. Lett.* **79**, 2225–2228 (1997).

[121] H. Gauck, M. Hartl, D. Schneble, H. Schnitzler, T. Pfau, and J. Mlynek, "Quasi-2D Gas of Laser Cooled Atoms in a Planar Matter Waveguide", *Phys. Rev. Lett.* **81**, 5298–5301 (1998).

[122] T. Seideman, "New Means of Spatially Manipulating Molecules with Light", *J. Chem. Phys.* **111**, 4397–4405 (1999).

[123] M. K. Olsen, T. Wong, S. M. Tan, and D. F. Walls, "Bichromatic Atomic Lens", *Phys. Rev. A* **53**, 3358–3368 (1996).

[124] T. Pfau, Ch. Kurtsiefer, C. S. Adams, M. Sigel, and J. Mlynek, "Magneto-Optical Beam Splitter for Atoms", *Phys. Rev. Lett.* **71**, 3427–3430 (1993).

[125] Q. Li, G. H. Baldwin, H.-A. Bachor, and D. E. McClelland, "Variable Focal-Length Lens for Atoms", *J. Opt. Soc. Am. B* **13**, 257–267 (1996).

[126] B. A. Zon and B. G. Katsnel'son, "Nonresonent Scattering of Intense Light by a Molecule", *Sov. Phys. JETP* **42**, 595–601 (1976).

[127] J. Ortigoso, M. Rodrigues, M. Gupta, and B. Friedrich, "Time Evolution of Pendular States Created by the Interaction of Molecular Polarizability with a Pulsed Nonresonant Laser Field", *J. Chem. Phys.* **110**, 3870–3875 (1999).

[128] A. A. Radzig and B. M. Smirnov, *Reference Data on Atoms, Molecules, and Ions* (Springer, Berlin, 1985).

[129] J. R. Gardner, R. A. Cline, J. D. Miller, D. J. Heinzen, H. M. J. M. Boesten, and B. J. Verhaar, "Collisions of Doubly Spin-Polarized and Ultracold ^{85}Rb Atoms", *Phys. Rev. Lett.* **74**, 3764–3767 (1995).

[130] C. C. Tsai, R. S. Freeland, J. M. Vogels, H. M. J. M. Boesten, B. J. Verhaar, and C. J. Heinzen, "Two-Color Photoassociation Spectroscopy of Ground State Rb_2", *Phys. Rev. Lett.* **79**, 1245–1248 (1997).

[131] J. D. Weinstein, R. deCarvalho, T. Guillet, B. Friedrich, and J. M. Doyle, "Magnetic Trapping of Calcium Monohydride Molecules at millikelvin Temperatures", *Nature* **395**, 148–150 (1998).

[132] J. D. Weinstein, R. deCarvalho, K. Amar, A. Boca, B. C. Odom, B. Friedrich, and J. M. Doyle, "Spectroscopy of Buffer-Gas Cooled Vanadium Monoxide in a Magnetic Trapping Field", *J. Chem. Phys.* **109**, 2656–2661 (1998).

[133] H. L. Bethlem, G. Berden, and G. Meijer, "Decelerating Neutral Dipolar Molecules", *Phys. Rev. Lett.* **83**, 1558–1561 (1999).

[134] C. Cohen-Tannoudji, J. Dupont-Roc, and G. Grynberg, *Atom-Photon Interactions: Basic Processes and Applications* (Wiley, New York, 1992).

[135] J. Dalibard and C. Cohen-Tannoudji, "Dressed-Atom Approach to Atomic Motion in Laser Light: The Dipole Force Revisited", *J. Opt. Soc. Am B* **2**, 1707–1720 (1985).

[136] M. D. Crisp, "Adiabatic-Following Approximation", *Phys. Rev. A* **8**, 2128–2135 (1973).

[137] A. P. Kazantsev, G. A. Ryabenko, G. I. Surdutovich, and V. P. Yakovlev, "Scattering of Atoms by Light", *Phys. Rep.* **129**, 75–144 (1985).

Abstracts of Publications I–V

I. Deflection of two-level atoms by a pulsed standing wave with a pulse duration of a few nanoseconds is studied by using the density matrix formalism. The effect of the limited coherence time of the pulsed laser field on the momentum distribution of the deflected atoms is investigated. In particular, we determine the coherence time at which the deflection by a pulsed standing wave differs significantly from the zero relaxation case.

II. We study the deflection of sodium atoms by a resonantly tuned pulsed standing wave of high field intensity. The effects of the phase fluctuations of the laser field are determined by measuring the momentum distribution of the deflected atoms at intermediate coherence times. The experimental results are explained using a theoretical model based on the generalized density matrix formalism of two-level atoms.

III. Atomic motion in a pulsed evanescent wave, with a pulse duration on the order of the lifetime of the excited state, is calculated using the semiclassical Bloch-equation approach. The equations for the internal atomic motion are solved using two approximations based on high laser intensity and on slow atomic velocity. The center-of-mass motion in the field under the effect of the dipole force is subsequently determined by numerical integration. As an example, the calculations show that the maximum normally incident velocity allowing a sodium atom to be reflected is approximately 35 m/s when using a 10 MW/cm^2 laser pulse of 7 ns duration. Our results also demonstrate that the velocity distribution of the reflected atoms may considerably differ from the distribution of the incident atoms due to different deceleration and acceleration times in a short laser pulse. This effect may lead to an average slowing-down of the reflected part of a thermal particle beam.

IV. Reflection of neutral atoms and molecules by a pulsed standing wave with a duration on the order of nanoseconds is studied. It is shown that with a suitable choice of the laser parameter values, each period of the pulsed standing wave functions as an independent mirror thus providing a novel way to manipulate large samples of neutral gas-phase particles even with a single laser pulse. At moderate field intensities, the pulsed standing wave mirror would be directly applicable, e.g., for the manipulation of buffer-gas cooled molecules.

V. Reflection of thermal atoms by a pulsed standing wave with a duration in the nanosecond region is studied. Momentum distribution of the reflected atoms is determined by theoretical calculations based on the adiabatic atom-photon interactions. It is shown, that with a proper choice of the field intensity and the pulse duration the standing-wave pattern functions as a row of independent

atomic mirrors. At an optimum choice of the parameter values, the fraction of the elastically reflected atoms is more than 20 %. Furthermore, we show that the pulsed standing-wave mirror can be used to reflect thermal atoms and to manipulate their final momentum distribution. When using laser pulses with an intensity of several tens of MW/cm^3 tens of thousands of atoms can be reflected by a single laser pulse.